Tectonics®

RESEARCH ARTICLE
10.1029/2022TC007461

Key Points:

- Along the Apennines, the geometries of the surface and the style of deformation and exhumation resemble the geometries of the Moho
- The coupling between shallower and deeper geometries demonstrates that along the Apennines, different subduction dynamics are ongoing
- Respect to the orogenic divide, the Northern-Apennines geometries are asymmetric whereas the Central Apennines geometries are symmetric

Supporting Information:

Supporting Information may be found in the online version of this article.

Correspondence to:

R. Lanari,
riccardo.lanari@unifi.it

Citation:

Lanari, R., Reitano, R., Faccenna, C., Agostinetti, N. P., & Ballato, P. (2023). Surface and crustal response to deep subduction dynamics: Insights from the Apennines, Italy. *Tectonics*, *42*, e2022TC007461. https://doi.org/10.1029/2022TC007461

Received 15 JUN 2022
Accepted 12 FEB 2023

Surface and Crustal Response to Deep Subduction Dynamics: Insights From the Apennines, Italy

R. Lanari[1,2], R. Reitano[2], C. Faccenna[2,3], N. Piana Agostinetti[4,5], and P. Ballato[2]

[1]Department of Earth Sciences, University of Florence, Florence, Italy, [2]Department of Science, Roma Tre University, Roma, Italy, [3]GFZ-German Research Centre for Geosciences, Potsdam, Germany, [4]Department of Earth and Environmental Sciences, Milano, Italy, [5]Osservatorio Nazionale Terremoti, Istituto Nazionale di Geofisica e Vulcanologia, Rome, Italy

Abstract The topography of orogenic belts responds to several contributions operating at short and long temporal and spatial (i.e., wavelengths) scales, from the surface to the deep mantle. Here, we aim to investigate the connection between morphometric characteristics, exhumation, and crustal deformation along and across the Italian Apennines, by comparing superficial with deeper data. Specifically, we present four sets of observations that are constructed by gathering previous data and adding new analyses and inferences, that include: (a) a new geomorphological set of analyses; (b) a database of available low temperature thermochronological cooling ages; (c) a reconstruction of drainage divide evolution in time and space based on the age of the youngest lacustrine deposits within each extensional basin; (d) Moho depth from receiver functions, gathering previous estimates and 13 new ones. From these sets of data, it emerges that across the main drainage divide of the Apennines, the morphological characteristics, the style of deformation and the spatial distribution of exhumation correlate with the geometries of the Moho and are associated with a strong asymmetry in the Northern-Apennines and a clear symmetry in the Central-Apennines. We interpret these results as evidence of a strong coupling between shallower and deeper geometries, that are most likely related to complex along-strike variations in the Apennines geodynamic setting.

1. Introduction

Mountain belts result from the interaction between surface, crustal, and deep mantle processes (e.g., Faccenna et al., 2014). The Apennines of Italy represents an ideal setting to investigate the possible linkage and feedback reactions between these processes. Several studies attempted to decipher these interactions by comparing the topographic elevation and the position of the orogenic drainage divide with the crustal thickness, the tectonic regime (e.g., compression and extension), the temperature at the Moho depth and the short-term vertical and horizontal motions (i.e., GPS; Diaferia et al., 2019; Faccenna et al., 2014; Faccenna & Becker, 2020; Gvirtzman & Nur, 2001; Miller & Piana Agostinetti, 2012; Piana Agostinetti & Faccenna, 2018; Rosenbaum & Piana Agostinetti, 2015; Savastano & Piana Agostinetti, 2019; Wortel & Spakman, 2000; Carminati & Doglioni, 2012; D'Agostino et al., 2001; Piana Agostinetti & Faccenna, 2018; Rosenbaum & Piana Agostinetti, 2015). Some of these works showed that the northern Apennines and the Calabrian arc, where subduction processes are still active, are characterized by a dynamically depressed topography due to downward pull (Figure 1, Carminati et al., 2005, 2010; Diaferia et al., 2019; Faccenna et al., 2014; Faccenna & Becker, 2020). There, the vertical motion estimated by GPS, integrated over a broad region, indicates subsidence (see Carminati et al., 2005; Faccenna et al., 2014). Moreover, in the northern Apennines, the topographic crest coincides with the orogenic drainage divide, which in turn overlaps with the transition between the western retro-wedge dominated by normal faulting, and the eastern pro-wedge characterized by thrust faulting (e.g., Carminati & Doglioni, 2012; D'Agostino et al., 2001). Conversely, in the Central and Southern Apennines, where subduction processes are inactive and slab break-off is thought to have occurred during the last 2.5 Ma, the high topography is not entirely compensated at depth by a crustal root, resulting in a positive residual topography. There, ongoing uplift is also demonstrated by vertical movements estimated by GPS (Figure 1; Serpelloni et al., 2013; Faccenna et al., 2014; Faccenna & Becker, 2020). This topographic signal is also accompanied by a positive thermal anomaly at Moho depth, showing higher temperatures beneath the wedge compared to the surroundings sections of the Apennines (e.g., Chiarabba & Chiodini, 2013; Diaferia et al., 2019 and reference therein). Moreover, in the Central Apennines, the orogenic drainage divide is shifted westward with respect to the highest topographic elevation and does not overlap with the transition between the extensional western retro-wedge and the contractional eastern pro-wedge as observed for the Northern Apennines (Bartolini et al., 2003; D'Agostino et al., 2001).

10.1029/2022TC007461

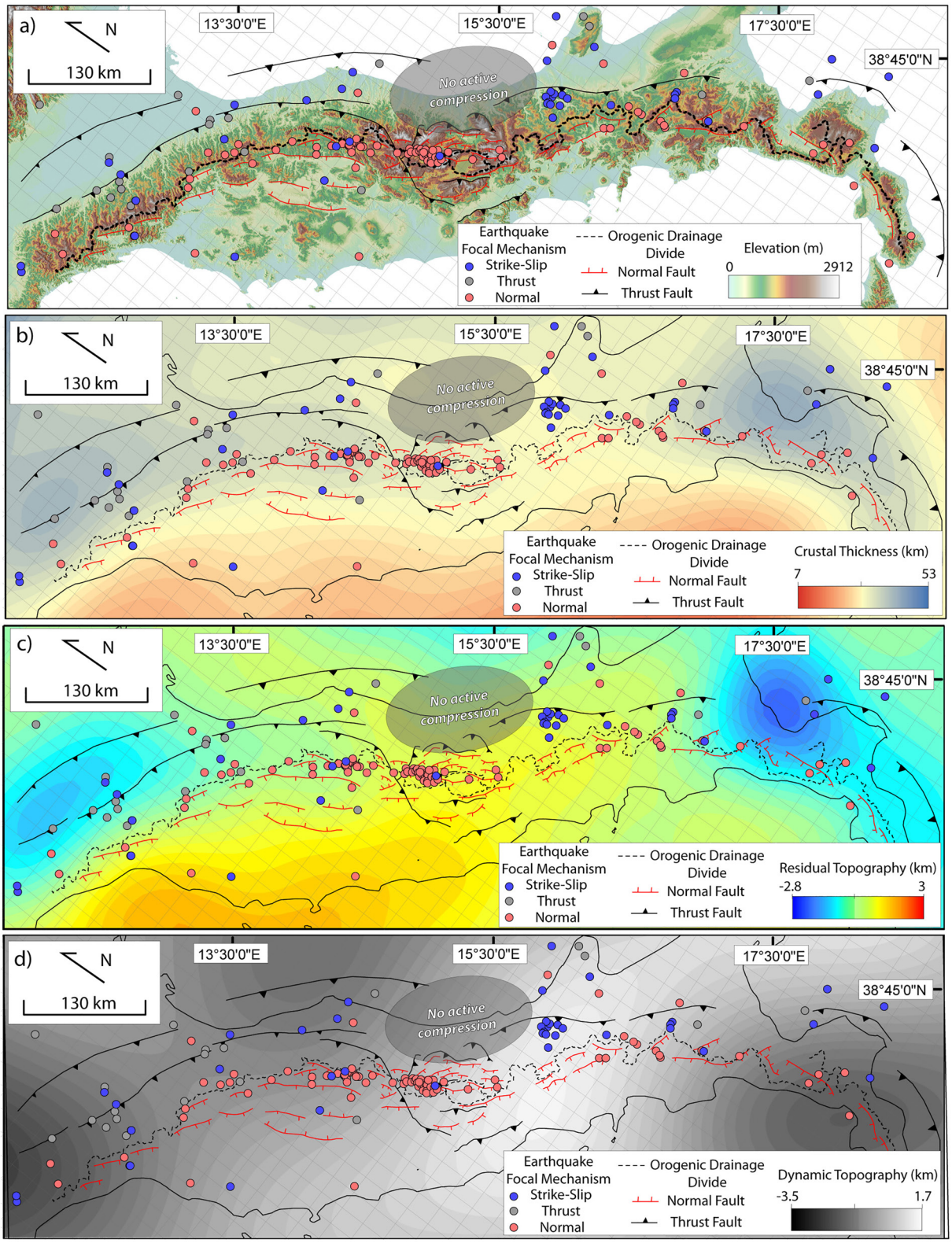

Figure 1. (a) topographic map of the Italian Peninsula. Earthquake focal mechanism from Montone et al. (1999), (2004), and (2012) and reference therein; (b) Crustal thickness (data from Faccenna & Becker, 2020); (c) residual topography (data from Faccenna & Becker, 2020); (d) Dynamic topography (data from Faccenna & Becker, 2020). For each map the traces of the main thrust and normal faults are drawn together with the orogenic drainage divide.

These works highlight the occurrence of a significant along-strike variability in geomorphologic and topographic characteristics, style of tectonic deformation, crustal architecture and mantle structure and raise major research questions: does such a variability correlate with different crustal and deeper processes or does it reflect lithological variations and/or major differences in rock erodibility and/or surface processes? How do crustal or mantle processes affect the tectonic regime and in turn the morphometry of the orogen? If crustal or mantle processes exert a major control on the surface characteristics of the orogen, can we potentially invert topography for understanding deeper structures?

To answer these questions, we combined available information with new data to obtain four independent datasets that provide new insights into the surface morphology, the magnitude and timing of exhumation, the Moho geometry, and the evolution of the orogenic drainage divide through time. Specifically, we present:

1. A new set of geomorphological analyses at the orogenic scale including topographic swath profiles, k_{sn} and χ maps. We use such analyses to describe the shape of the orogen and to qualitatively infer the across-divide pattern of uplift.
2. A database of available apatite fission tracks (AFT) and apatite (U-Th-Sm)/He (AHe) cooling ages covering the entire Apennines. We used low temperature thermochronology data to deduce the across-divide magnitude and spatio-temporal pattern of exhumation.
3. A new compilation of the ages of the youngest lacustrine deposits within the extensional basins along the Apennines. Such deposits, that indicate a low energy environment, are generally used to constraints the timing of the last internal drainage episode of the basin. Such an assumption allows us to restore a potential orogenic drainage divide back in time.
4. A compilation of the Moho depth estimates from receiver functions, gathering previous data and 13 new estimates beneath the Central Apennines. We used receiver function to describe the geometry of the crust.

Our analyses show that the topography, style of deformation, and pattern of exhumation across the Apennines systematically correlates with the geometry of the Moho. This allows recognizing a general asymmetry in the Northern Apennines and a symmetry in the Central Apennines from the surface (i.e., the topographic shape) to the Moho (i.e., depth and geometry). In addition, our findings suggest that in the Northern Apennines, local faulting and crustal isostasy exert a primary control on the topography, morphology of the landscape and position of the orogenic drainage divide. Conversely, in the Central Apennines, the topography and the drainage divide evolution appear to be mainly governed by mantle dynamics.

2. Structural and Geodynamic Setting of the Apennines

The Apennines evolution is related to the subduction of dense oceanic and continental lithosphere. The subduction kinematics resulted in the migration of the trench-arc-back arc system across the western and central Mediterranean. Specifically, from 30 to 15 Ma, the Western Mediterranean subduction system migrated southward leading to slab roll-back (Dewey et al., 1973, 1989; Faccenna et al., 1997, 2007; Gueguen et al., 1998; Malinverno & Ryan, 1986; Patacca et al., 1993; Royden, 1993; Wortel & Spakman, 2000). This triggered compression in the pro-wedge and extension in the retro-wedge, that is to say in the eastern and western flanks of the Apennines, respectively (Bennett et al., 2012; Chiarabba et al., 2005; Doglioni et al., 1999; Gutscher et al., 2006; Minelli & Faccenna, 2010). The retro-wedge extension led to the development of east- and west-dipping normal faults, which created marine and terrestrial intermontane basins (e.g., Angelica et al., 2013; Bennett et al., 2012; Cavinato & Celles, 1999; D'Agostino et al., 2001, 2011). These retro-wedge normal faults and extensional basins present an overall younging eastward trend from offshore to the inland sectors of the Italian peninsula (Carminati et al., 2004; Collettini & Barchi, 2004; Collettini et al., 2006; Cosentino et al., 2010; Papani et al., 2002; Patacca et al., 1993). The exception to this pattern is represented by the Central Apennines where inland normal faults do not record such an eastward rejuvenation, but rather a synchronous initiation at about 2.5 Ma (Cosentino et al., 2017).

Today, the slab that formed the Apennines accretionary wedge can be traced beneath most of the western Mediterranean region because it is marked by a horizontal high-P-wave speed layer in the mantle transition zone (MTZ) (Faccenna et al., 2014; Panza et al., 2007; Piromallo & Morelli, 2003; Wortel & Spakman, 2000; Zhu et al., 2012). However, due to the limited resolution and the relevant smearing effects on images obtained with seismic tomography at such a regional scale, the Apennines slab can be robustly imaged at depth up to ~300 km

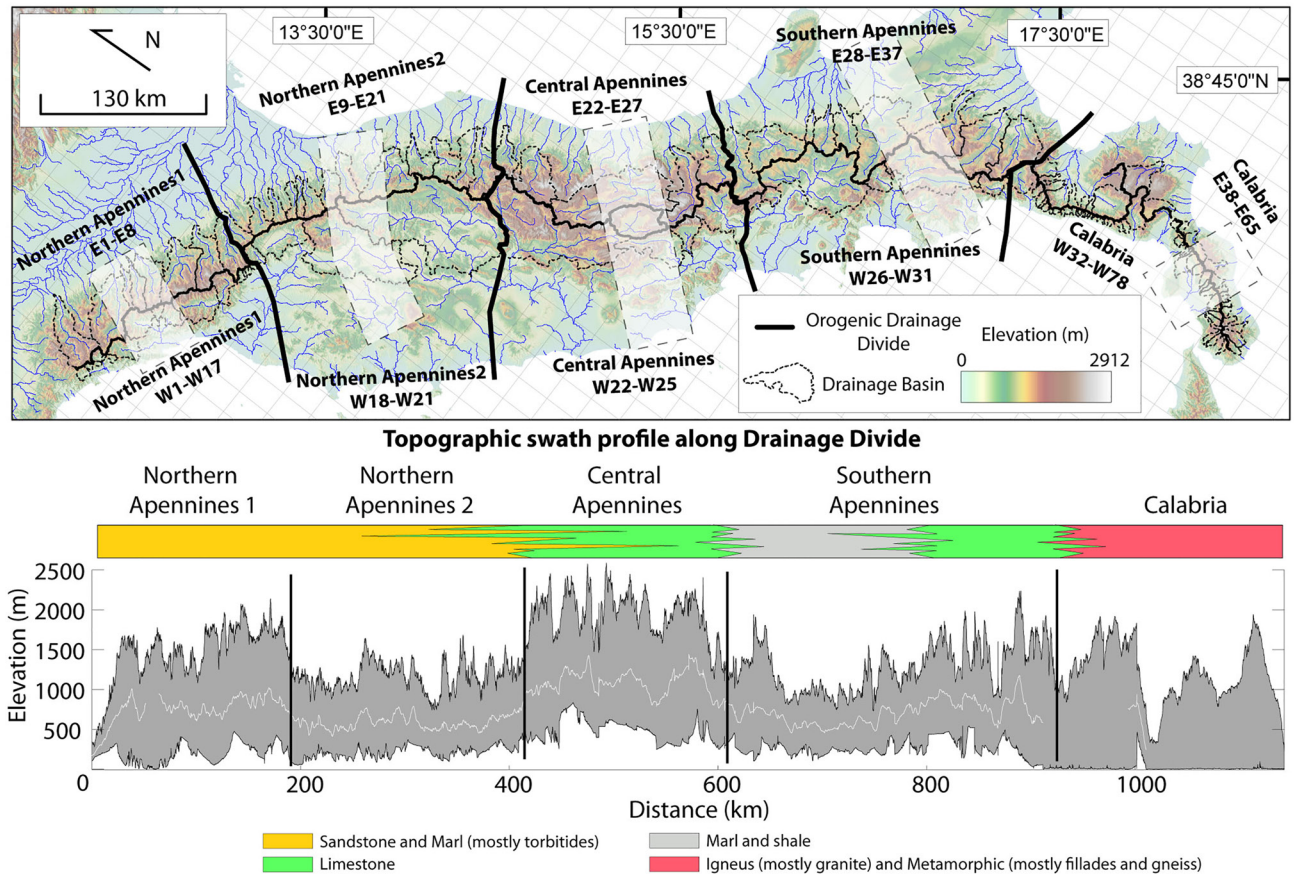

Figure 2. Topographic map of the Italian peninsula with river network in blue. Dashes black lines are the river catchments analyzed in this work while the thicker solid line is the orogenic drainage divide. White transparent boxes are swath profiles shown in Figures 9–13 (exception is from the Calabria Profile which is in Figure S1 in Supporting Information S1). In the lower part a topographic swath profile along the orogenic drainage divide with a schematic bar where the main lithology is shown.

(Benoit et al., 2011). The presence of a stagnant slab at the MTZ could be clearly inferred only for the Southern Tyrrhenian subduction zone (i.e., in front of the Calabrian arc) from the presence of deep earthquakes (focal depths larger than 300 km, Chiarabba et al., 2005). The continuity of the slab at depth in other portions of the Apennines subduction zone is more speculative. The absence of deep seismicity beneath the Northern Apennines (De Luca et al., 2009) is strong evidence against such a continuity. Moreover, beneath the Central and Southern Apennines, intermediate-depth seismicity, that is, with focal depth between 30 and 100 km, is also absent (Cimini & Marchetti, 2006), supporting the hypothesis of the presence of a 300-km-wide slab window. Such a slab window develops between depths of ∼70–∼100 km, suggesting an early stage of slab break-off (Faccenna et al., 2014; Gvirtzman & Nur, 1999, 2001; Wortel & Spakman, 2000), and further documents the heterogeneity of the Apennines subduction zone. The presence of a break in the slab is supported by: (a) the occurrence of a shallow slab gap as documented by seismic tomography; (b) the lack of deep seismicity (>30 km) (Chiarabba et al., 2005; Serpelloni et al., 2013); (c) the absence of active compressional deformation, as documented by Lower Pleistocene deposits sealing the frontal thrust faults (Casero, 2004; Chiarabba et al., 2005, 2010, 2014; Faccenna et al., 2014; Giacomuzzi et al., 2012; Gvirtzman & Nur, 2001; Lucente et al., 1999; Piromallo & Morelli, 2003; Wortel & Spakman, 2000); (d) the absence of earthquakes with compressional focal mechanisms (Figure 1a, blue dots; Montone et al., 1999, 2004, 2012). Thus, the Apennines can be subdivided along strike into three main domains: (a) the active northern Apennines, where continental subduction is taking place; (b) the active Calabrian subduction zone, where the Ionian Oceanic lithosphere sinks beneath Eurasia; (c) the inactive Central/Southern Apennines where slab break-off suppressed subduction processes.

1. The Northern Apennines show a mean moderate/low topographic elevation (Figure 2; <1 km) with a slightly negative residual topography of −200/−300 m and a relevant crustal thickness of up to 40 km (Figure 1; e.g.,

Di Stefano et al., 2011; Panza et al., 2007; Piana Agostinetti & Faccenna, 2018). Positive residual topographic anomaly is only recognized in the western back-arc regions (Faccenna & Becker, 2020; Figure 1).

2. The Calabrian arc presents a mean low topographic elevation (Figure 2; <1 km) with a slightly negative residual topography of −200/−300 m, a negative dynamic topography (Faccenna & Becker, 2020; Faccenna et al., 2014), and a crustal thickness of up to 50 km (e.g., Agostinetti et al., 2009; Piana Agostinetti & Amato, 2009). Shallow crustal thickness and slightly positive residual topography is only present in the active volcanic arc, onshore Calabria in the Tyrrhenian Sea (Figure 1).
3. The Central Apennines show the highest topography (Figure 2; >1 km) and a shallower Moho (up to ∼35 km) (Miller & Piana Agostinetti, 2012). This configuration results in a positive residual topography of ∼400 m, and a positive dynamic topography of almost the same amplitude (Faccenna et al., 2014; Faccenna & Becker, 2020; Figure 1).

3. Topographic Setting of the Apennines

The Italian Apennines and the Calabria arc show elevation up to 3 km (Central Apennines). On a 50 km wide swath profile (Figure 2), running across the orogenic drainage divide, the Apennines can be classified into five distinct sectors according to the distribution of the maximum elevations and the topographic characteristics (Figure 2). These sectors have been named as: Northern Apennines 1, Northern Apennines 2, Central Apennines, Southern Apennines, and Calabria. The "Northern Apennines 1" have a mean elevation of up to 900 m with a few mountain peaks higher than ∼2 km, and a topographic relief up to ∼1.8 km (Figure 2). The "Northern Apennines 2" have a mean elevation up to 700 m, with maximum peaks of ∼1.5 km, and a topographic relief up to ∼1.3 km. The "Central Apennines" have the highest mean elevation of the whole Apennines (up to 1.2 km) with several mountaintops over 2 km (and two summits of ∼3 km) and a topographic relief up to ∼2 km. The "Southern Apennines" present a gradual southward increase in the mean topographic elevation (from ∼500 to ∼800 m), in the elevation of the highest peaks (from ∼1 km to more than ∼2 km), and in the topographic relief (from less than ∼700 m to almost 2 km). Finally, the Calabrian arc comprises only the Calabria region and has a narrow width that locally is lower than the size of the swath profile of 50 km.

4. Methods

4.1. Morphometric Analysis

Morphometric analyses are extensively used as a proxy to infer the short-term landscape evolution and to detect variations in uplift rates or climatic conditions through time (e.g., D'Alessandro et al., 2003; Ferrarini et al., 2021; Lanari et al., 2022; Pazzaglia & Fisher, 2022; Piacentini & Miccadei, 2014; Picotti et al., 2009; Reitano et al., 2022). The relationship between the slope of a river and its drainage area is usually expressed by a power-law formulation known as Flint's law

$$S = k_s A^{-\theta} \tag{1}$$

where S is the topographic slope, A is the upstream drainage area, k_s is the steepness index, and θ is the concavity index (Flint, 1974). Since k_s and θ are correlated, k_s is usually normalized (k_{sn}) using a reference concavity index (θ_{ref}). Similarly, for fluvial networks that show exposed bedrock at the base, the erosion rate is commonly expressed as a detachment-limited stream power law (e.g., Whipple & Tucker, 1999)

$$E = K S^n A^m \tag{2}$$

where K is the bedrock erodibility that depends on the climatic condition, lithology, and channel geometry, and m and n are positive exponents (e.g., Goren et al., 2014). In the assumption of steady state conditions between erosion rate and uplift rate ($E = U$, Willett & Brandon, 2002), the elevation variability of a point of the Earth surface in time is zero: $\frac{dz}{dt} = U - E = 0$. Since E can be expressed as in Equation 2, we obtain

$$U - K S^n A^m = 0 \tag{3}$$

Solving for the slope we obtain

$$S(x) = \left(\frac{U}{K}\right)^{\frac{1}{n}} A(x)^{-\frac{m}{n}} \tag{4}$$

Comparing this equation, with Equation 1, we note that $k_s \sim \left(\frac{U}{K}\right)^{\frac{1}{n}}$ and $\theta \sim \frac{m}{n}$. We can correct the rivers longitudinal profiles for the area distribution, obtaining straight line instead of concave shapes, to highlight features such as structural of lithological variations in the river profiles. To do so, it is possible to integrate the previous equation over x (Willett et al., 2014), obtaining

$$z(x) = z(xb) + \left(\frac{U}{K \cdot A_0^m}\right)^{\frac{1}{n}} \int_{xb}^{x} \left(\frac{A_0}{A(x)}\right)^{\frac{m}{n}} dx \tag{5}$$

This latter equation can be treated as a straight line, since $z(xb) = q$, $k_{sn} \sim \left(\frac{U}{K \cdot A_0^m}\right)^{\frac{1}{n}} = m$, and $\chi = \chi(x) = \int_{xb}^{x} \left(\frac{A_0}{A(x)}\right)^{\frac{m}{n}} dx = x$. Elevation z is now a function of x above the sea level z(xb) and of a reference drainage area $\frac{A_0}{A_0}$, and river profiles are transformed into straight line using the integral term $\chi = \chi(x) = \int_{xb}^{x} \left(\frac{A_0}{A(x)}\right)^{\frac{m}{n}} dx$. From Equation 4, it follows that for the same bedrock erodibility, higher k_{sn} values indicate higher uplift rates, while assuming for the same uplift rate, higher k_{sn} values indicate higher bedrock erodibility (e.g., Kirby & Whipple, 2012). In turn, since k_{sn} is the slope of the z-χ straight line, assuming the same K, steeper χ plots indicates higher uplift rates (Perron & Royden, 2013). As k_{sn}, χ is also extracted with a normalized concavity index (θ), that we impose equal to 0.45 (Wobus et al., 2006). For $k_{sn\chi}$ and χ calculation we use a critical area of 1 and 10 km^2, respectively. To exclude the role of ancient upstream flat surfaces not yet readjusted to the most recent uplift rate, we provide the most representative k_{sn} value for each drainage basin by calculating the peak of the distribution rather than the average.

We describe the large-scale morphometry of the Apennines, both along and across strike, by performing a new morphometrics analyses that includes normalized steepness index (k_{sn}), drainage areas, longitudinal river profiles and χ plots from multiple river catchments (Kirby & Ouimet, 2011; Perron & Royden, 2013; Snyder et al., 2000; Willett et al., 2014; Wobus et al., 2006, 2010). River catchments were extracted from SRTM digital elevation models with 90 m resolution (downloaded from "https://srtm.csi.cgiar.org/srtmdata/"). This resolution can be considered acceptable given the large spatial scale of the work. Our analysis accounts only for catchments respecting the following conditions: (a) that base level is fixed at 100 m a.s.l.; (b) the orogenic drainage divide is included in each basin divide. River analyses are sensitive to the selection of the base level that frequently corresponds to the sea level, or the elevation of a lake or major trunk rivers, or the transition between the foreland basin band the orogenic wedge (see Forte & Whipple, 2018). For the Apennines wedge, we choose a uniform base level at an elevation of 100 m because, for most of the catchments, this elevation represents the transition between the foreland and the orogenic wedge. Different drainage areas across the same portion of the Apennines that share the same orogenic divide and the same base level elevation, can be then used as a proxy, together with the swath profiles to describe the shape and morphology. It follows that, across the same portion of the drainage divide, smaller fluvial catchments A respect to the other side of the wedge, would automatically imply a steeper topographic flank, because of Equation 1.

We analyze 78 basins draining the (western) retro-wedge up to the Tyrrhenian Sea and 65 basins draining the (eastern) pro-wedge up to the Adriatic and the Ionian Seas (Figures 3 and 4).

4.2. Low-Temperature-Thermochronology Database

Low-temperature thermochronology is a powerful tool to untangle exhumation histories of crustal blocks and thrust sheets. In this paper, we aim to illustrate the exhumational pattern, gathering the available cooling ages for the entire Apennines into a new compilation. A similar approach has been already proposed in other orogenic wedges, where it has provided insights into the spatial-temporal pattern of exhumation (e.g., High Atlas of Morocco, Lanari, Faccenna, et al., 2020; Lanari, Fellin, et al., 2020; Eastern Cordillera of Colombia, Siravo et al., 2018; Alborz of Northern Iran, Ballato et al., 2015; Apennines Abbate et al., 1994; Erlanger et al., 2022; Thomson et al., 2010; or at the scale of the Mediterranean Lanari et al., 2023). The Apennines are a relatively young orogen, where suitable lithotype rocks for this technique are mostly represented by Miocene siliciclastic turbidites (flysch). These deposits are generally a few km thick so that (U-Th)/He on zircons (ZHe), one of

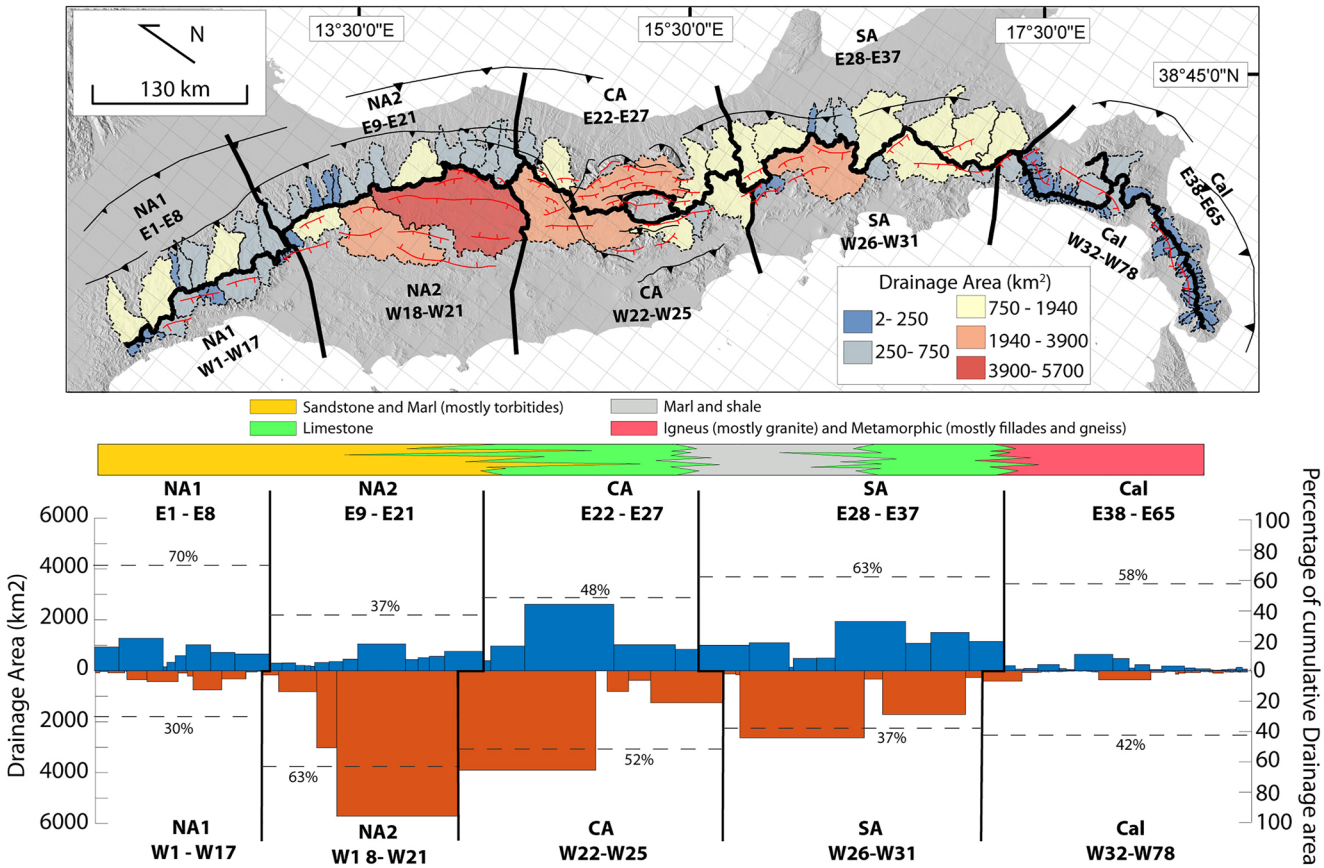

Figure 3. Hill-shade of the Italian peninsula where each river catchment (see Figure 2 for details) is labeled within discrete drainage area interval. In the lower part, the schematic bar where the main lithology is shown together with the histogram of the absolute drainage area value for each catchment, including the percentage of the cumulative drainage area for each region: NA1 (Northern Apennines 1), NA2 (Northern Apennines 2), CA (Central Apennines), SA (Southern Apennines), Cal (Calabria).

the deepest low-temperature-thermochronological system, is unsuited to detect exhumation processes. A few exceptions are represented by the Alpi Apuane, in the retro-wedge of the Northern Apennines, where middle crustal rocks have been exhumed (Balestrieri et al., 2003). Thus, our compilation includes only apatite (U-Th)/He (AHe; closure temperature of ~60°C; (Farley, 2000)) and apatite fission track (AFT; mean closure temperature of 110 ± 10°C; Green et al., 1989) data. The compiled ages with associated information are provided in Supporting Information S1, while the spatial distributions of the AHe and AFT cooling ages are shown in Figure 5. Following Thomson et al. (2010), in the Northern Apennines we selected 10 and 8 Ma for the AFT and AHe system, respectively, as a cooling age threshold for discriminating reset from partially to non-reset ages. In the Central/Southern Apennines, we considered a younger threshold of 6 Ma for both thermochronological systems because the depositional age of the preserved flysch units is slightly younger than that one of the Northern Apennines. Non-reset ages are shown in Figure 5 because they provide the maximum magnitude of exhumation (<~2 km and <~4 km for the AHe and the AFT system, respectively, assuming a geothermal gradient of 25°C/km and a mean surface temperature of 15°C), although they do not give information on the timing of exhumation and associated rates.

4.3. Receiver Functions Database

The receiver function method aims to isolate tele seismic P- to S-wave conversions associated with crust and mantle teleseismic discontinuities close to the receiver (Langston, 1979). Moho depth is computed from the time-delays of the P-to-s (Ps) converted at the Moho discontinuity and the associated reverberated phases between the free-surface and the Moho itself (PpPs, PsPs, and PpSs phases). Given an average crustal Vp value, couples of Moho depth and average crustal Vp/Vs ratio are tested in a grid-search to find the couple that theoretically produces arrival times of such phases closely matching the observations. This method is a fundamental tool to

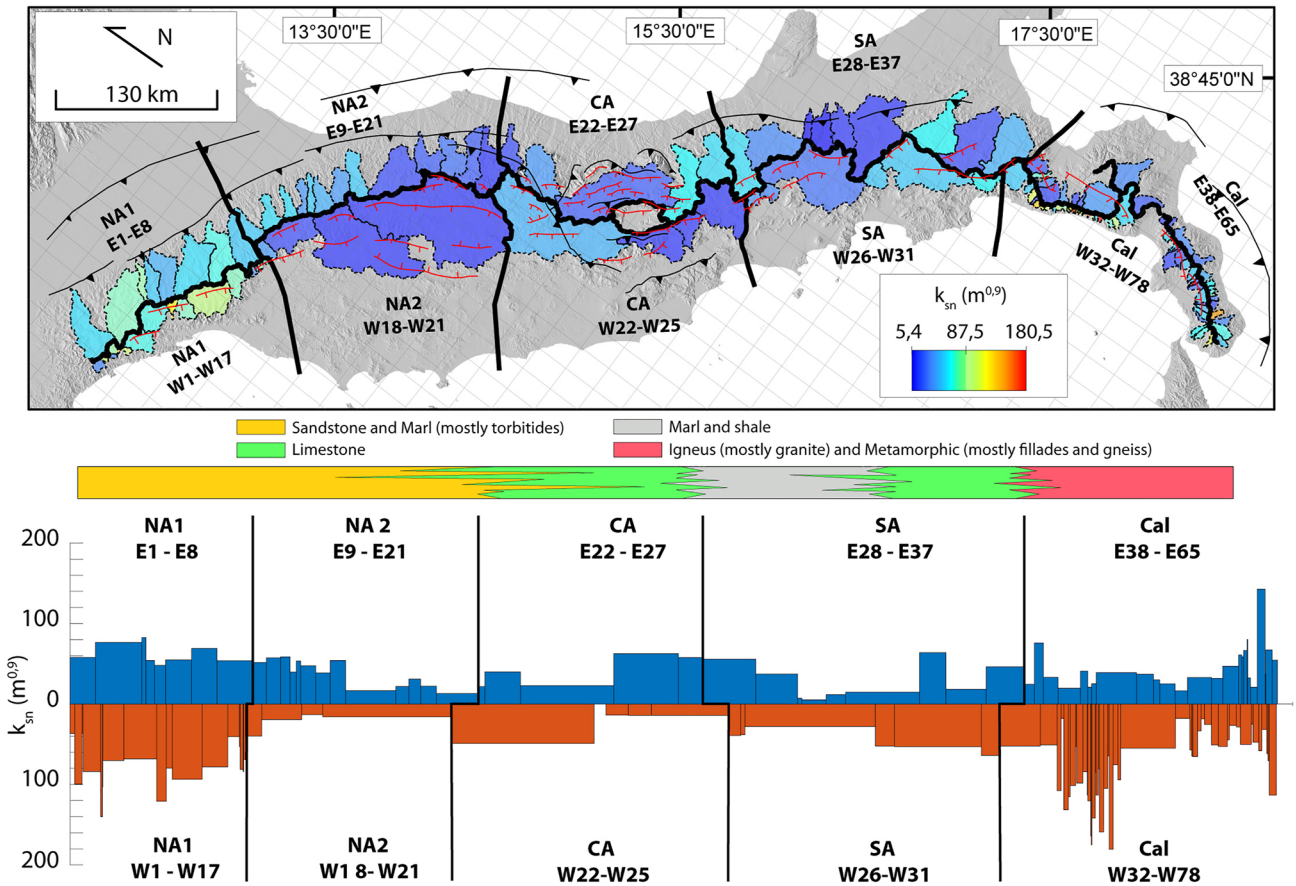

Figure 4. Hill-shade of the Italian peninsula where each river catchment (see Figure 2 for details) is labeled within discrete k_{sn} interval. The k_{sn} represent the pick of frequency for each basin (see main text for details). In the lower part, the schematic bar where the main lithology is shown together with the histogram of the absolute the k_{sn} value for each catchment.

estimate the Moho depth with a higher precision respect to any other geophysical investigations such as gravity surveys (Carannante et al., 2013). Along the Apennines, a large amount of Moho depth estimates was already published (Di Bona et al., 2018; Miller & Piana Agostinetti, 2012; Piana Agostinetti et al., 2009, 2022; Piana Agostinetti & Faccenna, 2018; Savastano & Piana Agostinetti, 2019) together with some compilations at the scale of the entire Apennines (Miller & Piana Agostinetti, 2012; Piana Agostinetti & Amato, 2009). Here, we compile all of them together with 13 new Moho depth estimates coming from stations located exclusively in the Central Apennines.

4.4. Lacustrine Deposit Database

A tectonic basin can be either internally drained (endorheic) with a local base level at any elevation, or externally drained (exorheic) with a base level that is generally the sea or a local base level such as a river that will flow into a larger water body. The endorheic-exorheic or exorheic-endorheic transition can occur during mountain building processes and are mainly controlled by the competition between the topographic growth of a divide (which in tectonically active areas is primarily function of faulting rate) and fluvial headward erosion (which depends on rock erodibility, precipitation and water discharge; e.g., Clementucci et al., 2022, 2023; Lanari et al., 2021). If the rate of topographic growth, and consequently the fault slip rate, is greater than the erosion rate, the basin develops as endorheic (Figure 7). Conversely, if fluvial incision is faster than the fault slip-rate, headward erosion will integrate the former endorheic systems into a larger, possibly exorheic fluvial systems (Figure 7). The internally drainage condition, especially for intermontane extensional basins, is generally not permanent and is commonly interrupted by a new capture from a nearby catchment. Conversely, the externally drainage configuration might persist for a longer time because once captured, the increased discharge makes the fluvial incision rates much

10.1029/2022TC007461

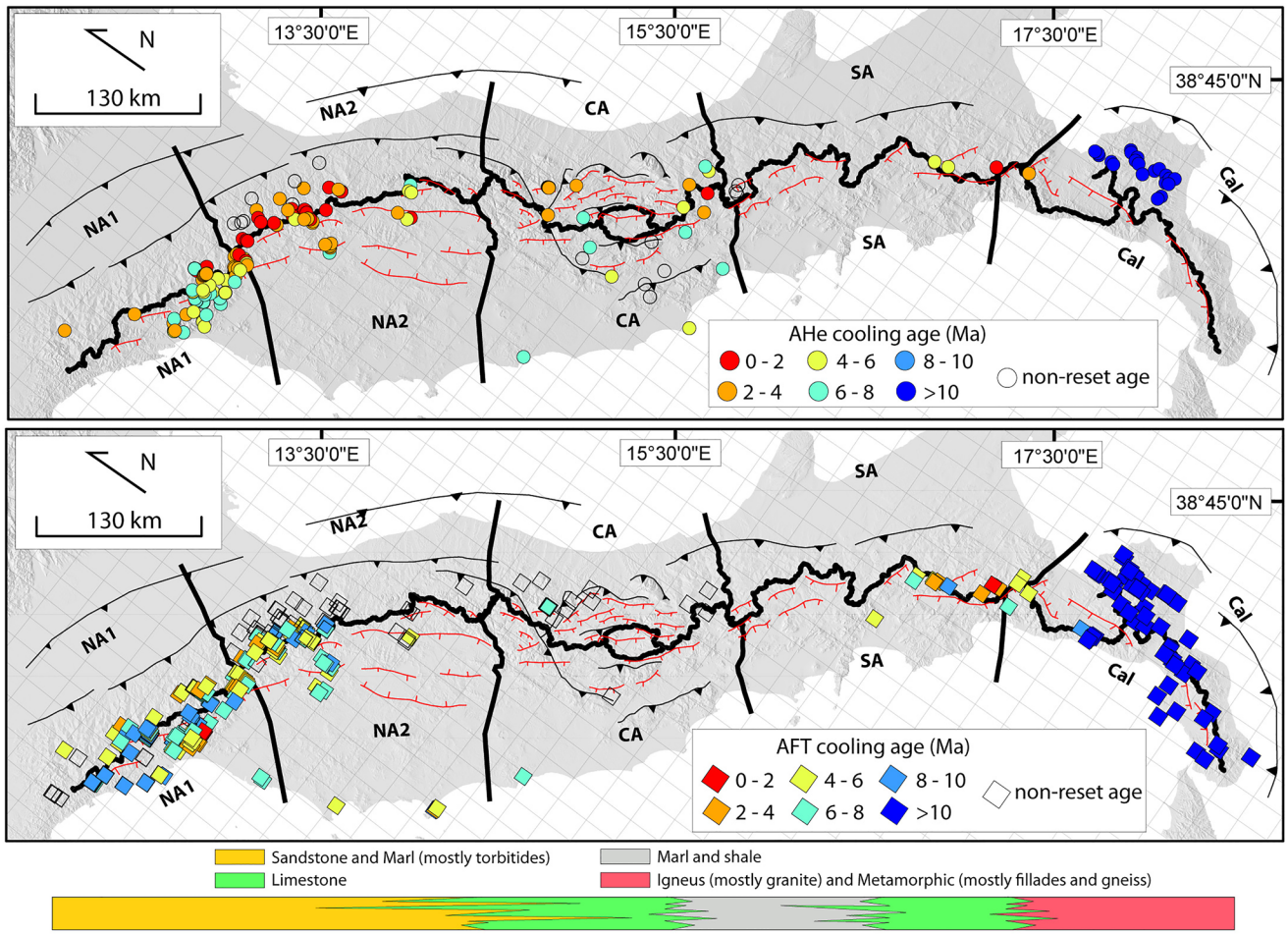

Figure 5. Hill-shade of the Italian peninsula with river catchments (see Figure 2 for details) together with (U-Th)/He (AHe) and apatite fission track ages (AFT) on apatite (see main text and Supporting Information S1 for references). In the map, no-filled symbols are ages that are not reset. Data From (Abbate et al., 1994; Balestrieri et al., 1996, 2011; Balestrieri & Ventura, 2000; Bonini et al., 2013; Carlini et al., 2013; Corrado et al., 2005; Fellin et al., 2007, 2021; Iannace et al., 2007; Invernizzi et al., 2008; Malusà & Balestrieri, 2012; Mazzoli et al., 2006, 2008, 2014; Olivetti et al., 2017; Rusciadelli et al., 2005; Thomson, 1994; Thomson et al., 2010; Ventura et al., 2001; Vignaroli et al., 2012; Zattin et al., 2002).

faster than the vertical movement along the faults (D'Agostino et al., 2001). The stratigraphic characteristics of the continental deposits filling the endorheic basins are a function of the tectonically generated accommodation space, the sediment supply and the availability of water, which depends on the ratio between water influx (i.e., precipitation and underground water discharge) and evaporation (Carroll & Bohacs, 1999). These characteristics can be inverted to unravel the dynamic evolution of the basins. Specifically, in case of endorheic systems, low energy deposits (e.g., shales or clays) are expected to lay in the basin depocenter even at high elevations as documented for high-altitude endorheic basins of the interior of orogenic plateaus (e.g., Tibet and Puna-Altiplano in South America). Conversely, when an endorheic basin is captured, fluvial incision and eventually deposition of coarse-grained deposits (e.g., conglomerates and sandstones) occurs. The time of transition from endorheic to exorheic conditions is commonly inferred by the age of the youngest lacustrine deposits that should approximate the last time span of internal drainage (Heidarzadeh et al., 2017).

In this sense, we compiled the youngest ages of the lacustrine deposits of each intermontane extensional basin along the Apennines to constraint the timing of the last endorheic phase. This timing and approach may encode information on the orogenic divide evolution (i.e., the hypothetical position back in time; Figure 8), especially for the basins located in the interior of the orogen, that otherwise are generally inferred by numerical codes (see He et al., 2021). Similar compilations have been already proposed for smaller spatial scale studies (e.g., Bartolini, 2003; Geurts et al., 2018). Our compilation includes 34 basins, that are listed in Supporting Information S1 (Table S4).

It should be noted that we exclude from the compilation older compressional basins (e.g., the Sant'Arcangelo and Del Taro thrust stop/piggy back basins) and we only account for the extensional ones. Moreover, we do not consider endorheic basins located at large distance from to the modern orogenic drainage divide, since their internal drainage conditions are likely supported by other processes (see for instance the Trasimento Lake, which is controlled by Quaternary topographic swelling due to the volcanic fields emplacement, e.g., the Amiata ridge; Bolsena volcanic field; e.g., Conticelli et al., 2015; Morroni et al., 2015). For such basins, the transition between internal and external drainage is not primarily controlled by the competition between faulting and river incision, as expected for the intermontane basins nearby the orogenic drainage divide.

4.5. Filtered Topography and Synthetic Orogenic Drainage Divides

The admittance analysis confirms the hypothesis that the large wavelength topography in the Apennines is dynamically supported by mantle (D'Agostino et al., 2001). The long wavelengths topographic signal can be directly imaged by filtering the topography at different wavelength. This can be done through a "circle average" consisting in averaging each pixel with circle areas with three different diameters of 50, 100 and 150 km (Figure 9). From the filtered topography is possible also to extract the synthetic divide, (see also Molin et al. (2012) and Moodie et al. (2018)). If the large wavelength synthetic drainage divide matches the actual one, it is then possible to deduce that the actual topography is likely sustained by mantle. On the other hand, if local faulting or crustal isostasy control the topographic evolution, only short wavelength filtered topography, and its synthetic divide, is expected to resemble the modern one.

5. Data Analysis

5.1. Topography and Morphometric Characteristic

Figures 3 and 4 show the results of the drainage areas and the normalized steepness index (k_{sn}) analysis, respectively. River catchments are labeled according to discrete intervals. There, we separated the eastern from the western basins through a horizontal line, which represents the orogenic drainage divide. The horizontal width of each box is proportional to the orogenic drainage divide portion bounding each basin, while the height of the box represents the drainage area of the basin (Figure 3b) and the k_{sn} value (Figure 4b). In this concern, it is worthwhile to highlight that due to the presence of a large internally drained basin in the Central Apennines (the Fucino Basin), we added a gap along the western divide which is shorter than the eastern divide (Figures 3 and 4).

The river catchments with the largest drainage area are in the Northern Apennines 2 (up to 5,000 km^2), and in the Central and the Southern Apennines (up to 4,000 km^2 for both regions), whereas the Calabrian block presents the smallest fluvial basins (up to 500 km^2). The highest k_{sn} values (i.e., the highest peak values for each basin) are instead in Calabria (up to 200 $m^{0.9}$) and in the Northern Apennines 1 (up to 150 $m^{0.9}$), while the Northern Apennines 2, the Central and the Southern Apennines exhibit k_{sn} never exceeding 80 $m^{0.9}$. Specifically, the Northern Apennines 1 present the smallest basins with the highest k_{sn} in the western flank (retro-wedge), whereas the Northern Apennines 2 exhibit the smallest basins, with the highest k_{sn}, in the eastern flank (pro-wedge). Conversely, the Central and Southern Apennines are rather symmetric with river catchments of similar dimensions and comparable k_{sn} across the drainage divide. Finally, the southwestern sectors of the Calabrian block are rather symmetric with small basins and moderate k_{sn} on both flanks, while its northeastern sectors are gently asymmetric with smaller, basins and higher k_{sn} along the western wedge.

5.2. Timing and Rates of Exhumation

In this section, we discuss only fully reset cooling ages of each sector as specified in the methods (Figure 5). In the Northern Apennines 1, AHe cooling ages vary between 1.2 ± 0.7 and 8.1 ± 0.5 Ma, while AFT ages range from 2.6 ± 0.5 to 11.2 ± 1.3 Ma. In the Northern Apennines 2, AHe cooling ages vary between 2.3 ± 0.1 and 9.5 ± 0.7 Ma, while AFT cooling ages vary from 3.6 ± 0.5 to 11.6 ± 1.4 Ma. In the Central Apennines, single grain AHe ages range from 1 to 109 Ma, and AFT central ages range from 5 ± 1.7 to 25 ± 13 Ma. In the Southern Apennines, the great majority of the AFT cooling ages are fully reset and range between 9.2 ± 1.0 and 1.5 ± 0.8 Ma, while all AHe ages are reset and range from 5.9 ± 0.6 to 1.6 ± 0.9 Ma. The Calabrian arc presents the oldest cooling ages of the entire Apennines. Only three AFT cooling age are younger than 12 Ma giving ages

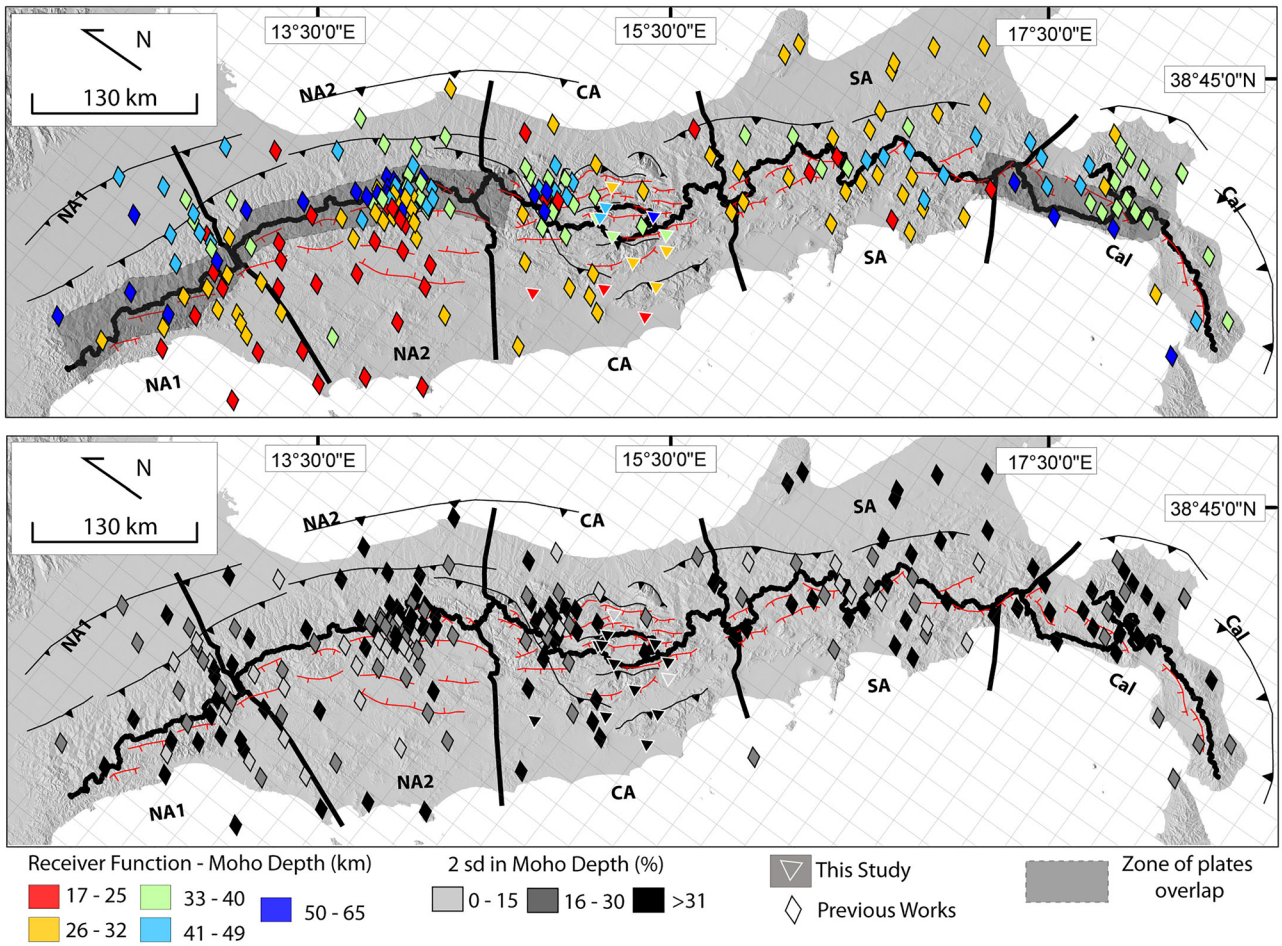

Figure 6. Hillshade of the Italian peninsula with Moho depth estimation form receiver function data base. Diamonds with black outline are data from literature (see main text and Supporting Information S1 for references) and diamonds with white outline are new stations. In the lower map is shown the error (2 sd express in percentage respect to the Moho depth estimation) associated to the single estimation.

of 5.1 ± 1.0 Ma, 7.2 ± 1 Ma, 6 9.5 ± 1.0 Ma, while only two AHe cooling ages are younger than 12 Ma (3.7 ± 0.2 and 9.1 ± 0.8 Ma).

5.3. Moho Depth Variations Along Strike

Our new and published receiver functions indicate that the crustal thickness of the Italian peninsula ranges between ~17 and ~65 km (Figure 6). Overall, we recognize four different domains of similar characteristics including: (a) the eastern pro-wedge with a ~35 km deep Moho; (b) the western retro-wedge with a shallow Tyrrhenian Moho that generally does not exceed ~25 km of depth; (c) the axial orogenic sectors of the Northern Apennines 1 and 2 and Calabria where the eastern Adriatic/Ionian Moho overlaps with the Tyrrhenian one reaching values up to 58 km; and (d) the axial orogenic sectors of the Central and Southern Apennines where an almost flat Moho at a depth of 45 km (just excluding four estimations) can be followed from the Adriatic to the Tyrrhenian coast.

5.4. Potential Orogenic Drainage Divide Restoration Back in Time

The youngest lacustrine deposits preserved in the extensional sedimentary basins of the Apennines have an age ranging from 5,000 years to 8 Ma (Figure 8). Overall, these ages become younger at increasing elevation while approaching the orogenic drainage divide. In the northern Apennines 1 and 2, the transition from endorheic to exorheic conditions occurred only in the western retro-wedge suggesting that the orogenic divide migrated

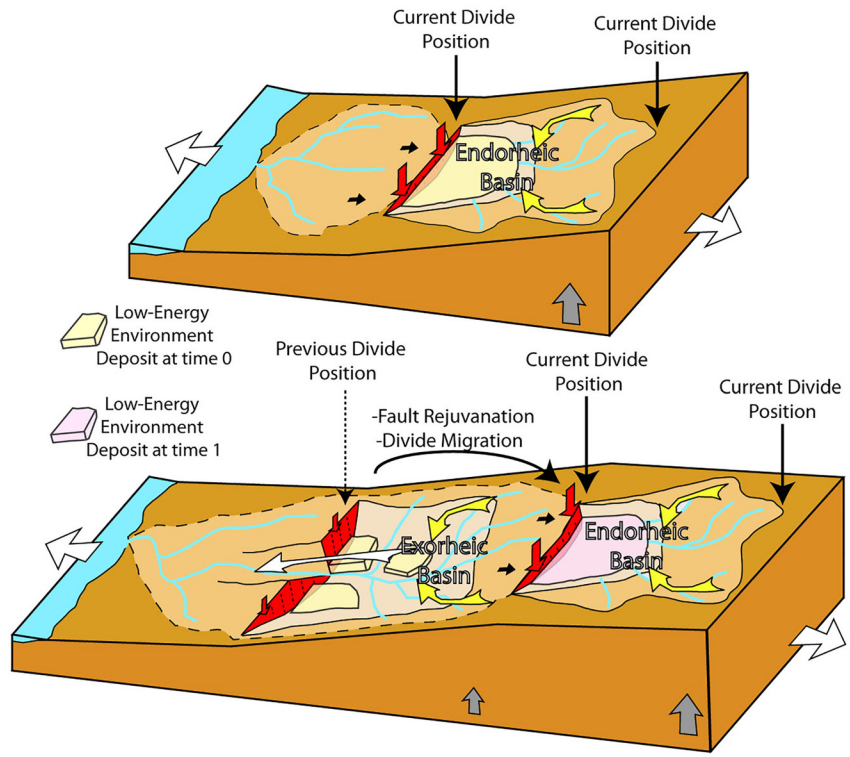

Figure 7. Conceptual model for endorheic-exorheic and exorheic-endorheic transition for small intermontane basins (modified after Lanari et al., 2021).

only eastward. Moreover, in the Northern Apennines, divide migration processes occurred from the Tortonian (Volterra Basin) up to early Pleistocene (e.g., Gubbio, San Sepolcro or Mugello basins). Finally, in the Northern Apennines 1, there no basin was capture after the middle Pleistocene. Conversely, in the interior of the Central and Southern Apennines, the transition from endorheic to exorheic conditions occurred on both sides of the orogen suggesting that the drainage divide migrated at the same time eastward and westward toward the axial zone. Finally, in the Central and Southern Apennines, divide migration has mostly started since the late Pliocene/early Pleistocene, and hence more recently than in the northern ones.

5.5. Comparison Between Synthetic and Orogenic Divides

Figure 9 shows three different filtered topographic maps at wavelengths of 50, 100 and 150 km together with the associated synthetic drainage divides and their along-strike distances from the current one. In the northern Apennines 1, the synthetic divides at increasing wavelengths discords from the current divide, laying further east, whereas in the Northern Apennines 2 it is located further west. Along these sectors, the modern position of the orogenic drainage divide only overlaps with the short-wavelength synthetic divide (e.g., 50 km filtering; Figure 9a blue line). Conversely, in the Central and Southern Apennines, the synthetic divides, at all investigated wavelengths, generally overlap with the current one.

6. Discussion

In this work we aim to explore if the surface morphology and the crustal deformation pattern reflect crustal and/or deeper mantle geometries. To achieve this goal, we: (a) describe the different and independent datasets along four representative cross sections (Sections 6.1. to 6.4); and (b) attempt to link the surface and crustal processes with the deep geodynamic mechanisms (Sections 6.5. to 6.6). For each sector we then provide a complete overview of the surface morphologies, the crustal exhumation, and the Moho geometry, together with the evolution of the orogenic drainage divide. Our analyses also include the Calabria sector, but according to the scope of this paper, it is excluded from the discussion because of its different tectonic setting (i.e., forearc of the Ionian oceanic subduction system) respect to the Apennines (i.e., accretionary wedge).

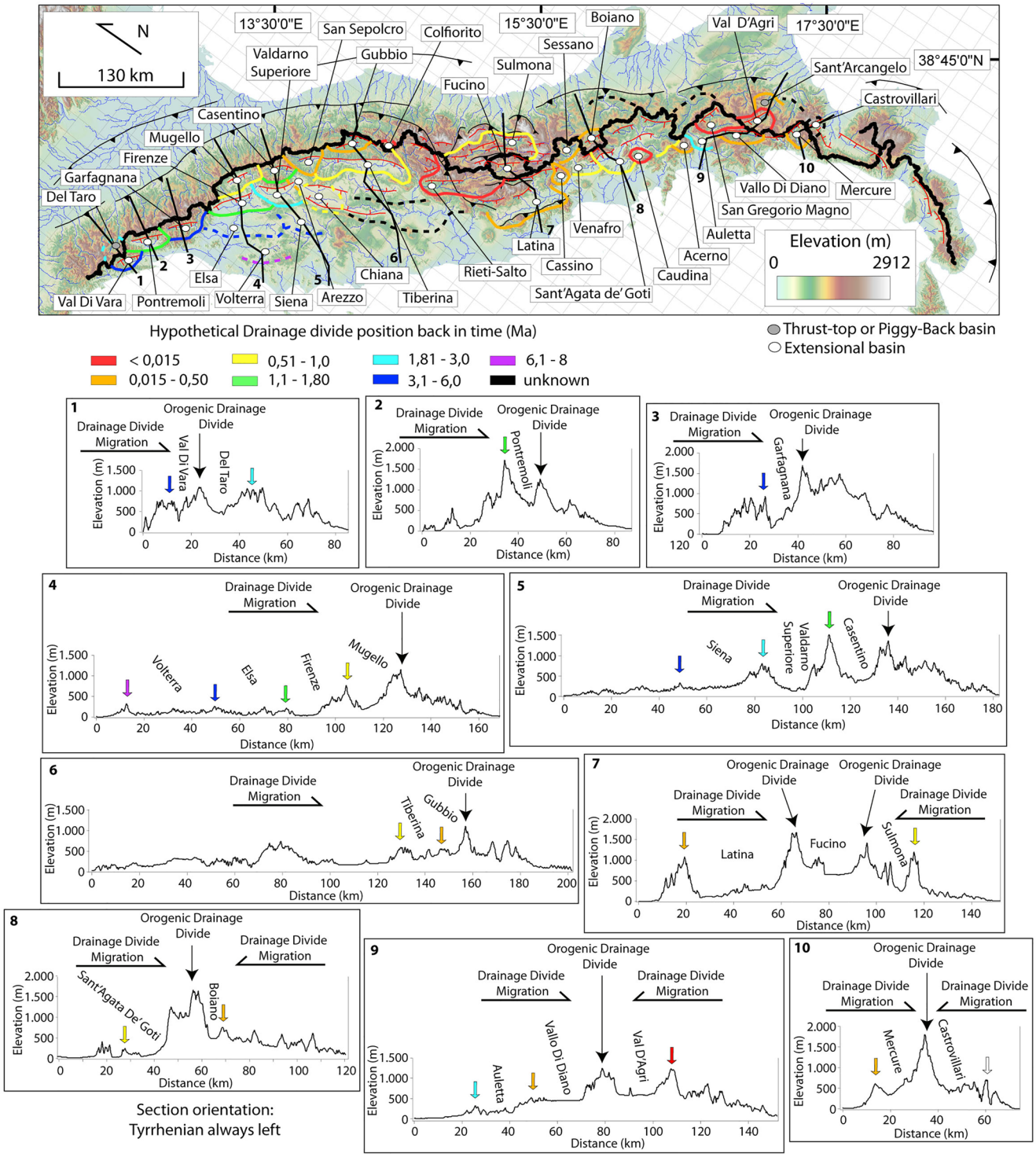

Figure 8. Topographic map of the Italian peninsula with the river network in blue. Thick black solid line is the orogenic drainage divide while thin black solid lines are the topographic sections which are shown in the lower part of the figure. Dashed colored lines are hypothetical drainage divide position back in time, labeled respect to the youngest lacustrine age reported for each previous endorheic basin. Solid colored lines are instead confident previous position of the drainage divide (see main text for details). White circles are extensional basins while gray circles are compressional basins. See main text and Supporting Information S1 for references. Data from (Amato et al., 2011, 2014; Bartolini, 2003; Basilici, 1997; Benvenuti, 2003; BERTOLDI, 1988; Bossio et al., 1994, 1995; Di Naccio et al., 2013; Ermolli et al., 2010; Ferreli et al., 1992; Ficcarelli et al., 1997; Fidolini et al., 2013; GHINASSI et al., 2005; Gioia et al., 2011; Ielpi, 2011; Mancini et al., 2020; Manzi et al., 2010; Martini et al., 2011; Pennetta et al., 2014; Peretto et al., 2015; Pucci et al., 2003, 2014; Sabato et al., 2005; Villani et al., 2015; Villani & Pierdominici, 2010; Zembo, 2010).

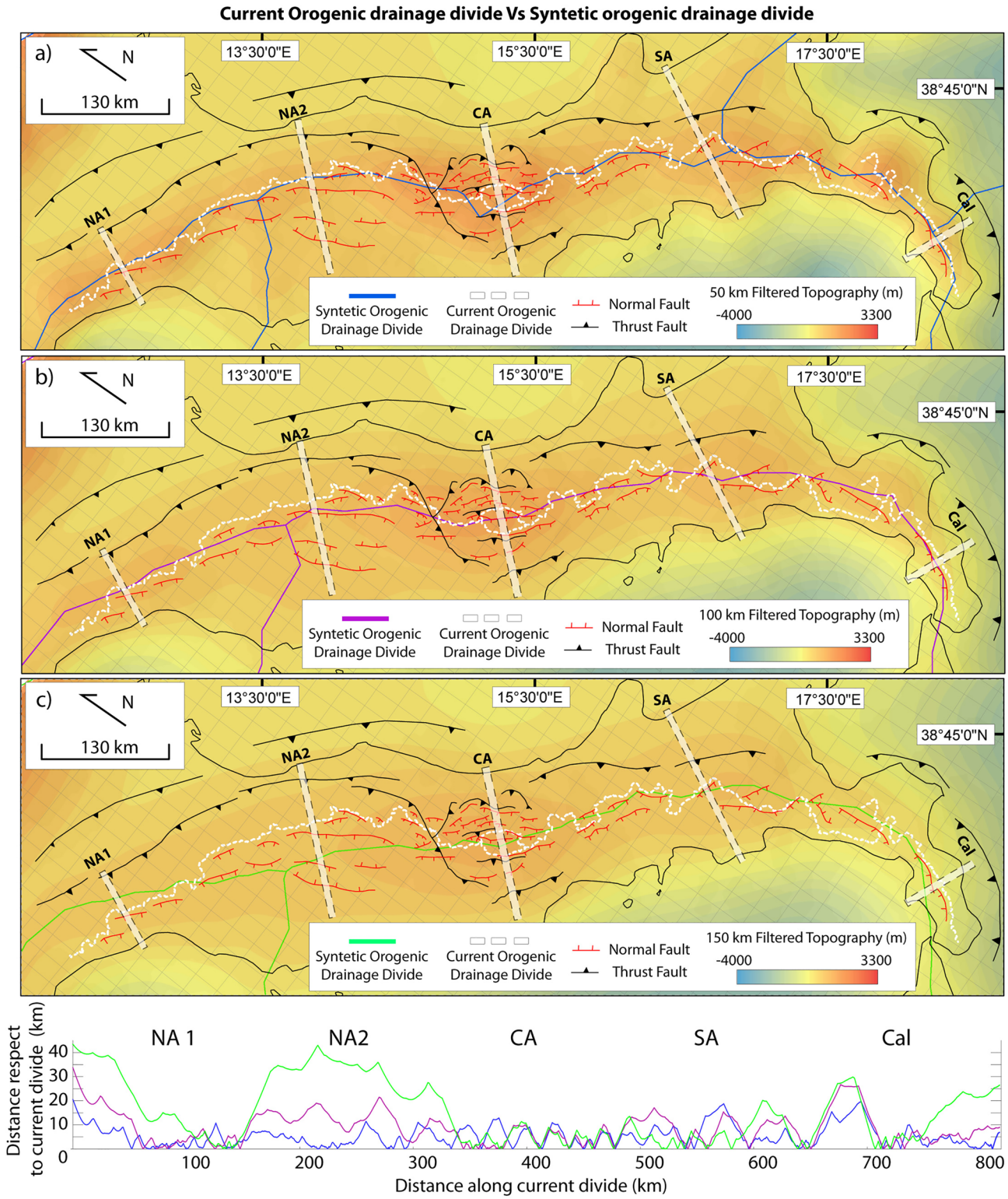

Figure 9. Three filtered topographic maps with increasing average window. (a) 50 km, (b) 100 km, and (c) 150 km. For each map the synthetic orogenic drainage divide position is located (see main text for details) together with the current orogenic drainage divide (dashed white line) and normal and thrust faults are shown. White transparent boxes are the profiles shown in this Figure and Figures 10–13 (exception is from the Calabria Profile which is in Figure S1 in Supporting Information S1). At the bottom, graphic displaying along divide, the horizontal distance between each synthetic orogenic drainage divide with the current orogenic drainage divide.

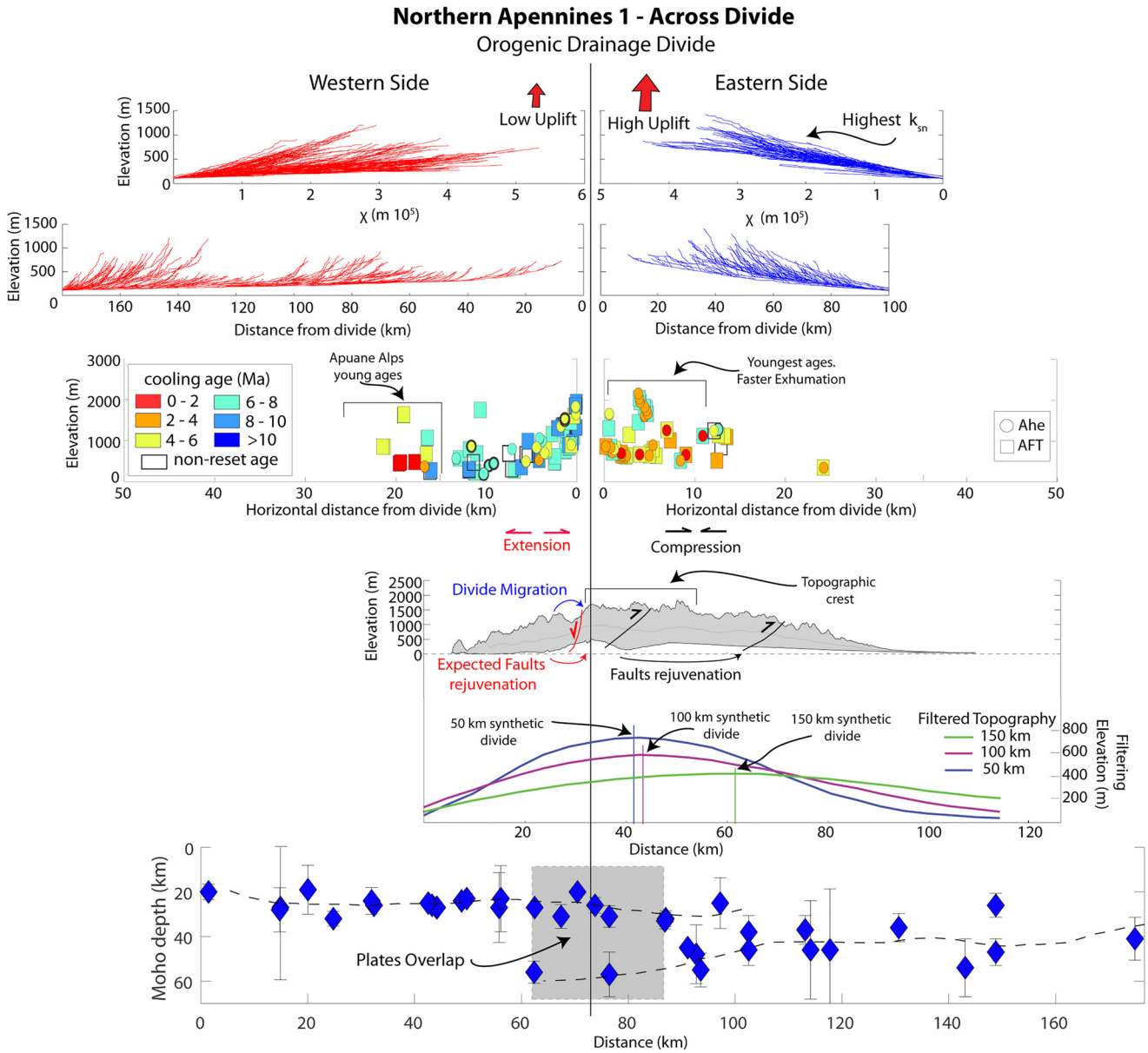

Figure 10. Northern Apennines 1 across-divide differences. Form top: chi and longitudinal river profiles from each basin (see main text for details; in red rivers draining toward west while in blue rivers draining toward east). Elevation Versus Horizontal distance from divide where cooling ages are plotted and labeled respect to the age (see main text for references). Topographic swath profiles (50 km of window) with position of the orogenic drainage divide and the main faults: normal in red and thrust in black. Moho depth Versus distance (see main text for references).

Importantly, we observe a correlation between the orogen along-strike lithological variations, and the morphological characteristics. However, the across-strike variations in lithology are rather limited and hence to a first approximation, we can conclude that the retro-wedge and the pro-wedge of each topographic sector have similar lithotypes. In the Northern Apennines 1 the dominating lithology is represented by well-stratified, coarse- to fine-grained turbidites, while in the Northern Apennines 2 the turbidites are associated with pelagic limestones within a southward increasing trend. The Central Apennines include shallow-water marine limestones and, to a lesser extent, pelagic limestones and turbidites, where the latter are mostly exposed within valleys. The Southern Apennines are composed of marls and shales in the northern part and limestone in the southern one. Finally, Calabria is mainly constituted by igneous and metamorphic rocks. It is worthwhile to consider that the along-strike lithological variations are not expected to control the along-strike morphological and structural variations. If this would be the case, across each

sector, where the lithology is similar (e.g., Northern Apennines 1 and 2), we should expect similar geometry and features.

6.1. Northern Apennines 1

The Northern Apennines 1 topographic swath profile (Figure 10) shows an asymmetric geometry with respect to the orogenic drainage divide, with the western side that is much steeper than the eastern one. Such a configuration is also suggested by the presence of fluvial catchments in the western flank that are smaller than those of the eastern one (Figure 3). Across the Northern Apennines 1, morphometric features also strongly change from east to west. Although the western basins have the highest k_{sn}, the χ slope is higher on the eastern side suggesting a non-uniform uplift rate, with faster uplift along the eastern side (Figure 10; Erlanger et al., 2022). This conclusion is justified by the occurrence of rocks across the divide with similar erodibility.

The asymmetric geometry at surface is also visible in the crustal structures. As observed by D'Agostino et al. (2001), the orogenic drainage divide overlaps with the transition between the compression in the eastern pro-wedge side and the extension in the western retro-wedge side (Figure 10). AFT and AHe cooling ages display a younging trend with increasing elevation, with the western flank presenting younger ages than the eastern one. In the pro-wedge, AFT and AHe cooling ages are both reset, suggesting a maximum amount of exhumation >3–4 km. Moreover, they are significantly younger compared to the western side, indicating faster exhumation in the pro-wedge (Figure 10; see also the compilation provided in Erlanger et al., 2022). This indicates that erosional exhumation associated with topographic growth induced by contractional deformation is more efficient that tectonic denudation driven by normal faulting. The only exception to this trend is in the Alpi Apuane, where young cooling ages are located at a long distance from the orogenic drainage divide. The interpretation of those ages is not straightforward although to a first order, exhumation appears to be driven by normal faults (Balestrieri et al., 2003).

The geometry of the Moho also reveals an asymmetric pattern. Across the Northern Apennines 1, Moho depth estimates show a gentle west-dipping Adria subducting plate beneath the pro-wedge, whereas to the west the Moho geometry is shallower and flat from the Tyrrhenian Sea to the Apennine wedge. The transition between the subducting and overriding plates is marked by a sector where shallow and deep Moho depth estimates coexist (Figure 10).

6.2. Northern Apennines 2

The Northern Apennines 2 topographic swath profile (Figure 11) shows an asymmetric geometry with respect to the orogenic drainage divide, with the eastern side being much steeper than the western one. This topographic asymmetry is also displayed by the morphometric parameters with smaller fluvial catchments (Figure 3), higher k_{sn} (Figure 3) and χ values along the eastern flank. Given the occurrence of similar lithologies on both orogenic sides, this configuration suggests that uplift is faster in the eastern flank (pro-wedge).

The asymmetry on the surface is also visible in the crustal structure with the orogenic drainage divide, coinciding with the transition between the compressional pro-wedge side to the east, and the extensional retro-wedge side to the west (Figure 11; D'Agostino et al., 2001). AFT and AHe cooling ages become younger at increasing elevation but considering the same altitude and distance from the orogenic divide, the ages differ between the pro-wedge and the retro-wedge. In the pro wedge of the Northern Apennines 2, at long distance from the divide, AFT are rarely reset, suggesting a maximum amount of exhumation <3/4 km, and are partially reset westward, approaching the orogenic divide. AHe are instead significantly young at short distance from the orogenic divide, suggesting fast exhumation rates during the last 2 Ma (Figure 11). Conversely, on the western side of the wedge, AFT cooling ages are reset, while the AHe tend to be 2 Myr older than those of the eastern flank. This indicates that there must have been a shift in the locus of faster exhumation. Prior to 2 Ma, exhumation was focused on the western flank where extensional tectonics dominates. From 2 Ma exhumation became more localized on the pro-wedge where contractional deformation and erosional unroofing prevails. This configuration is corroborated by the geomorphic parameters, which indicate faster uplift rates in the pro-wedge.

The geometry of the Moho also reveals a sharp asymmetry. Beneath the pro-wedge of the Northern Apennines 2, the Moho shows a steep west-dipping geometry related to the Adria subducting plate. Conversely, to the west, the Moho geometry is rather flat from the wedge to the Tyrrhenian Sea. As also noted beneath the Northern

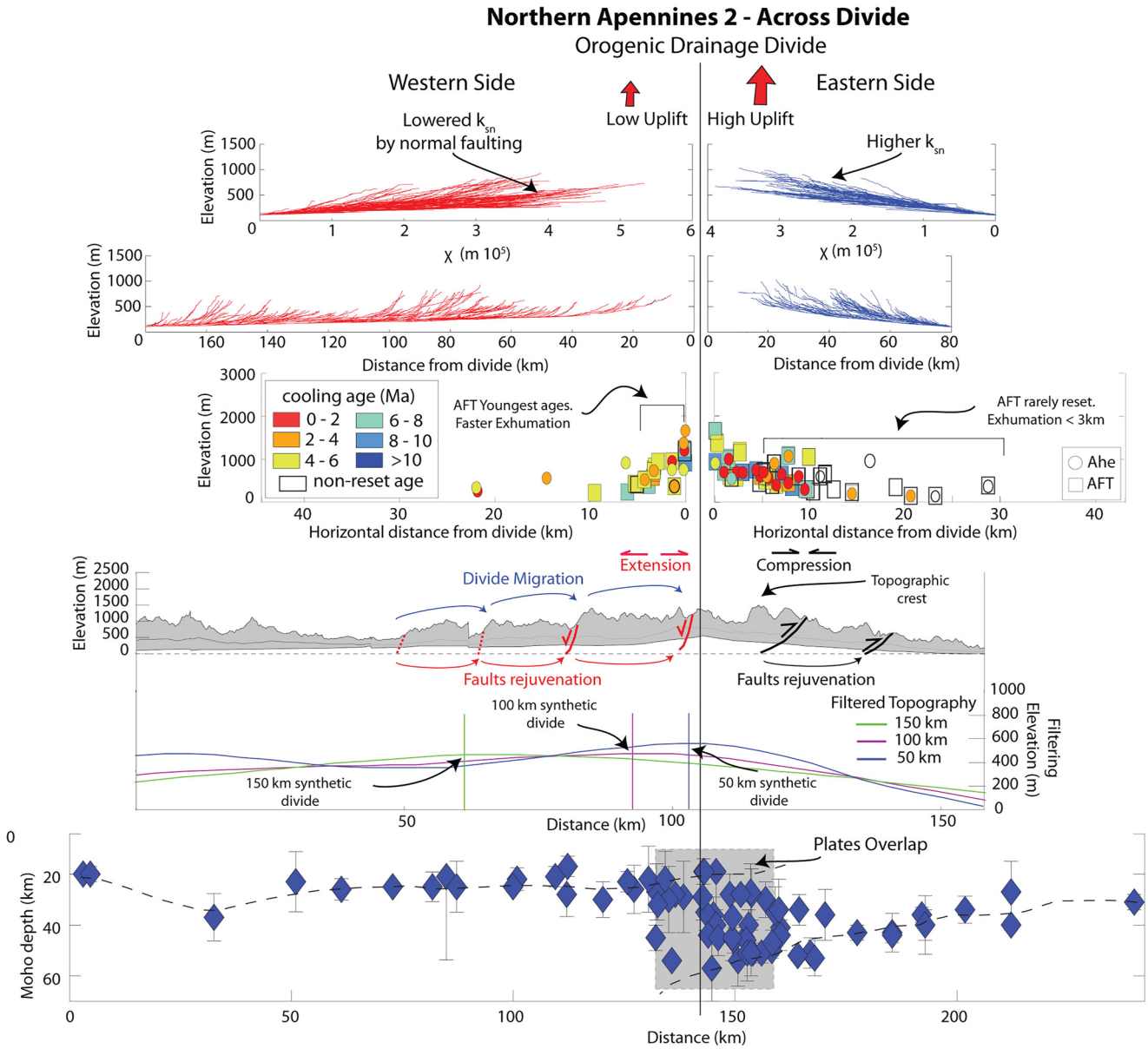

Figure 11. Northern Apennines 2 across-divide differences. Form top: chi and longitudinal river profiles from each basin (see main text for details; in red rivers draining toward west while in blue rivers draining toward east). Elevation Versus Horizontal distance from divide where cooling ages are plotted and labeled respect to the age (see main text for references). Topographic swath profiles (50 km of window) with position of the orogenic drainage divide and the main faults: normal in red and thrust in black. Moho depth Versus distance (see main text for references).

Apennines 1, the transition between the subducting and the overriding plates in the Northern Apennines 2 is marked by an area, where the shallow Tyrrhenian Moho overlaps with the deeper Adrian one.

6.3. Central Apennines

The Central Apennines topographic swath profile (Figure 12) shows an overall symmetric geometry with respect to the orogenic drainage divide, with the eastern and western flanks sharing a similar slope. The topographic symmetry is also displayed by the similar size of the fluvial catchments (Figure 3) and the topographic metrics with comparable k_{sn} and χ values (Figure 4) across the divide, indicating rather uniform uplift rates along both sides of the wedge. Again, this conclusion is supported by the presence of similar lithotypes across the divide.

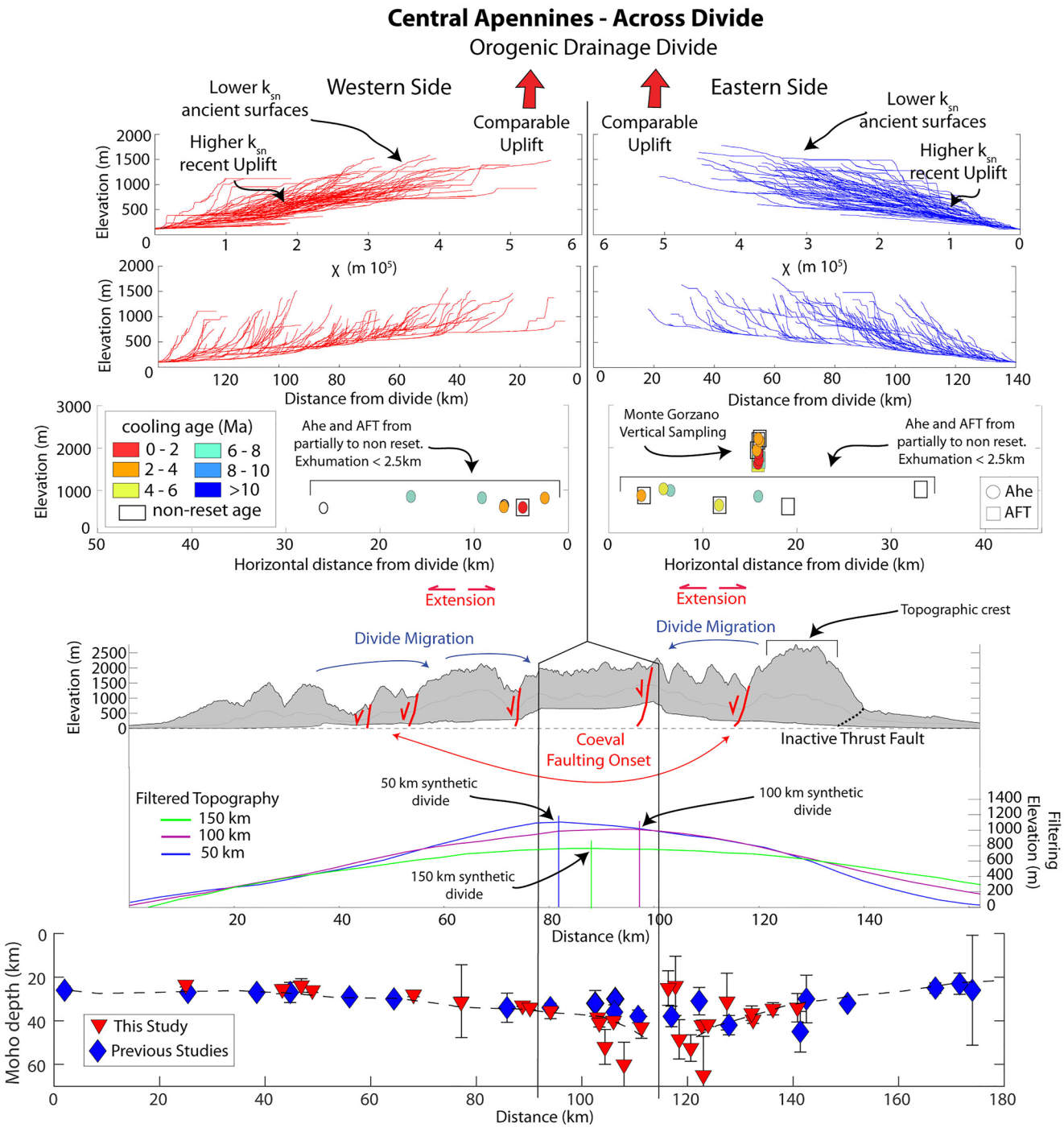

Figure 12. Central Apennines across-divide differences. Form top: chi and longitudinal river profiles from each basin (see main text for details; in red rivers draining toward west while in blue rivers draining toward east). Elevation Versus Horizontal distance from divide where cooling ages are plotted and labeled respect to the age (see main text for references). Topographic swath profiles (50 km of window) with position of the orogenic drainage divide and the main faults: normal in red and thrust in black. Moho depth Versus distance (see main text for references).

As mentioned in the background section (Section 2), in the Central Apennines compression likely vanished in the early Pleistocene (Casero, 2004; Cosentino et al., 2017). In the Central Apennines the orogenic drainage divide is located within the extensional domain of the axial zone, but normal faults occur in both, the western and eastern flanks (D'Agostino et al., 2001). AFT and AHe cooling ages are not abundant to appreciate age-elevation patterns because limestones represent the dominant lithology. Nevertheless, considering the elevation and the

10.1029/2022TC007461

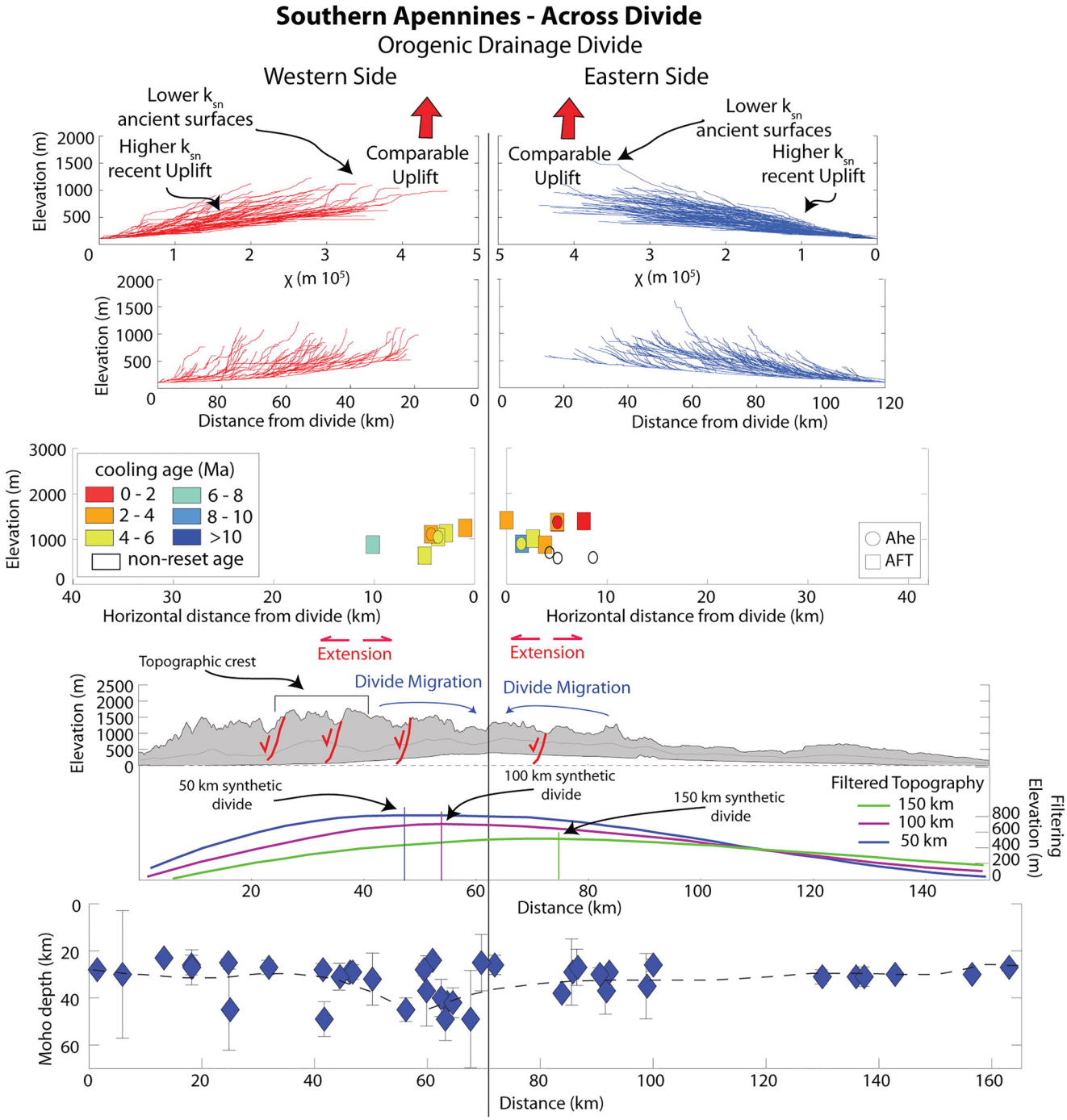

Figure 13. Southern Apennines 1 across-divide differences. Form top: chi and longitudinal river profiles from each basin (see main text for details; in red rivers draining toward west while in blue rivers draining toward east). Elevation Versus Horizontal distance from divide where cooling ages are plotted and labeled respect to the age (see main text for references). Topographic swath profiles (50 km of window) with position of the orogenic drainage divide and the main faults: normal in red and thrust in black. Moho depth Versus distance (see main text for references).

distance from the drainage divide the few data points on both flanks present similar ages. AFT ages are rarely reset, suggesting a maximum amount of exhumation lower than 3–4 km, while AHe are generally partially reset, suggesting <2 km of exhumation. The only exception to this pattern is in the eastern side of the wedge, and is related to the Monte Gorzano vertical profile that shows young ages (<4 Ma) at high elevation (Fellin et al., 2021).

Beneath the Central Apennines, the Moho appears to gently slope down into the mantle with a symmetric geometry (e.g., Miller & Piana Agostinetti, 2012; Piana Agostinetti & Amato, 2009; Piana Agostinetti et al., 2022).

6.4. Southern Apennines

In the Southern Apennines (Figure 13) the topography has a complex shape given the occurrence of the high-relief ridge (Cilento high) in proximity of the Tyrrhenian coast. Nevertheless, the mean topography shows an overall symmetric geometry (but not as evident as the Central Apennines) with respect to the orogenic drainage divide, with the eastern and western sides sharing a similar slope. Such a topographic symmetry is also evident in the size of the fluvial catchments (Figure 3), the topographic metrics k_{sn} (Figure 4) and the χ slope, which values are comparable for both flanks of the wedge suggesting uniform uplift rates across the orogenic divide (given the rather uniform, across-strike lithology).

This symmetric surface geometry mimics the pattern of the Moho. The Southern Apennines orogenic drainage divide is located within the region under extension with normal faults on both the western and the eastern flank. The density of AFT and AHe cooling ages is not sufficient to appreciate age-elevation patterns, although across divide they are comparable. AFT ages are reset suggesting a maximum amount of exhumation >3–4 km. AHe ages vary along strike with ages that are generally partially reset in the southern sector, suggesting moderate exhumation (<2 km), while they are non-reset in the northern sectors. The youngest cooling ages are from Monte Alpi and thermal modeling (Mazzoli et al., 2014), and indicate higher exhumation rates during the Pliocene-late Pleistocene.

Across the Southern Apennines, the geometry of the Moho is not easy to define but to a first approximation it reveals an overall symmetric pattern. It appears to be at the similar depths on both sides of the orogen (Savastano & Piana Agostinetti, 2019) with both sides gently sloping down into the mantle.

6.5. Coupling Between Surface and Deeper Processes

Our revised geophysical (Moho depth estimates) data, thermochronological (AFT and AHe ages) compilation, and morphometric (longitudinal river profiles, χ and K_{sn} plots) analyses reveal differences across and along the Apennine orogenic wedge. The cross sections in Figures 10 and 11 illustrate that in the Northern Apennines 1 and 2 the topography across-divide, together with trends in uplift rates and magnitude of exhumation, are consistent with the structural variations expected for a retro- and pro-wedge. Specifically, in the pro-wedge active thrusting drives topographic growth through crustal thickening at rates that are faster than those observed in the retro-wedge. Although higher uplift rates are expected to promote faster surface erosion as observed across the Northern Apennines 1, in the Northern Apennines 2 the long-term exhumation rates in the eastern pro-wedge are lower than in the western retro-wedge (compare AFT and AHe data of Figures 10 and 11). This pattern is most likely a result of tectonic denudation driven by normal faulting (e.g., Balestrieri et al., 2003; Thomson et al., 2010). Moreover, the reconstruction of the orogenic divide back in time documents an overall eastward divide migration. This is consistent with the ages of the opening of the endorheic extensional basins that rejuvenate eastward following the onset of extension (e.g., Bossio et al., 1995; Collettini et al., 2006). All these observations suggest that crustal processes (i.e., pro-wedge shortening vs. retro-wedge extension) may control the geometry of topography (Figures 10 and 11) in the Northern Apennines. Such an inference could be also deduced from the filtered topographies. Across the Northern Apennines 1 and 2, the short wavelength topography (e.g., 50 km, blue line Figures 10 and 11) strongly resembles the modern ones, while there are not similarities with the larger wavelength filtered topographies (e.g., 100 and 150 km, purple and green lines Figures 10 and 11).

Conversely, Figures 12 and 13 illustrate that across the Central and Southern Apennines there is an overall symmetrical distribution of topography, uplift and magnitude of exhumation. Even if it is unclear if compression along the frontal structures is still ongoing, the extensional domain is located further east with respect to the position of the orogenic drainage divide (i.e., in the pro-wedge). The orogenic divide reconstruction back in time reveals fluvial capture on both sides of the wedge, suggesting a bi-directional divide migration while, thermochronological cooling ages do not show variations across the Central Apennines indicating limited and slow exhumation on both sides of the wedge. Moreover, extension across the Central Apennines started almost simultaneously at about 2.5 Ma (Cosentino et al., 2017; Fisher et al., 2022). This implies that the Central Apennines and Southern Apennines do not show the eastward migration of the extensional domain as observed in

the Northern Apennines 2, at least over the Pleistocene. All these observations suggest that short wavelength processes (crustal processes-normal faulting) are not primarily affecting the exhumation pattern and in turn the geometry of the topography and the position of the orogenic drainage divide. We then suggest that a different process, which is likely deeper and with a larger wavelength with respect to the Northern Apennines, is controlling the geometry of topography across the Central and Southern Apennines. This inference is corroborated by the similarity between the across-divide profiles of the short and long wavelength topographies (e.g., 50, 100, and 150 km; Figures 12 and 13), that also resemble the profile of the present topography.

These observations and conclusions agree with those one from Pazzaglia and Fisher (2022) which derived the uplift history from fluvial catchments along the entire Apennines through the linear inversion of longitudinal river profiles. According to the pattern and rates of uplift, they suggest that an isostatically-driven uplift, in response to wedge shortening and thickening, controls uplift processes in the northern Apennine while in the Central Apennines uplift is most likely associated with a mantle-driven dynamics. In conclusion, our study supports previous observations, and their implications, concerning the position of the orogenic drainage divide, the topographic elevation peak, and the transition from retro-wedge extension to pro-wedge compression (D'Agostino et al., 2001; Carminati & Doglioni, 2012). Such a transition in the Northern Apennines overlaps with the orogenic drainage divide, while in the Central and Southern Apennines the transition is shifted eastward respect to the topographic crest (e.g., D'Agostino et al., 2001). In this context, our work provides a further observation, showing that in the Northern Apennines 1 and 2 the coincidence between the drainage divide, and the shift to the extensional domain is located above a region where the eastern plate subducts below the western one. Conversely, in the Central and Southern Apennines our Moho depth estimates confirm that there is no ongoing subduction and that the Adria and the Tyrrhenian plates gently and symmetrically flex down, beneath the topographic crest. Such an observation has a crucial implication because it indicates that the topography closely reflects the crustal geometry and its variation along strike from the Northern Apennines to Central-Southern Apennines.

6.6. Slab Roll-Back Versus Slab Break-Off: Effect on Crust and Topography

Here, we reconstruct the long-term surface and crustal evolution of two transects (Figure 14; Northern Apennines 2 and Central Apennines) according to the along-strike variation in geodynamic processes, from active subduction, in the Northern Apennines, to slab break-off in the Central Apennines. To reconstruct the hypothetical evolution of the Apennines, we combine the modern configuration of the wedge and the coupling between topography, and Moho position, together with the reconstruction of the divide migration and deformation back in time.

Across the Northern Apennines, both thrust fronts in pro-wedge and normal faults in the retro-wedge become younger eastward (e.g., Collettini et al., 2006; Coward et al., 1999). The eastward trend of normal faulting rejuvenation likely drops the slip rates of older normal faults, favoring river incision and basin integration and promoting the eastward migration of the orogenic divide (see also Section 4.4). This pattern is consistent with the eastward slab roll-back that enhance the outward (eastward) propagation of compression and extension. The present-day configuration with a strong coupling between surface, crust and Moho allow us to reasonably infer that in a previous stage of the evolution, the Northern Apennines should have been characterized by similar remarkably asymmetric patterns likewise the modern (Figure 14-stage 1). It is worthwhile to note that the velocity of slab roll-back significantly affects the geometry of the belt, which remains asymmetric. This is the case for the Northern Apennines 2 that differs from Northern Apennines 1 by a faster slab retreat velocity (Malinverno & Ryan, 1986; Royden & Faccenna, 2018). If the slab migration is faster, the retro wedge extension and associated crustal thinning will be much more developed with crucial effects on both topography and exhumation. The former will be lowered by normal faulting resulting in a gentle topographic flank in the retro-wedge, while the latter will be more impacted by tectonic denudation. This may explain why the retro wedge of the Northern Apennines 1 is steeper and has older cooling ages than the Northern Apennines 2.

Conversely, across the Central Apennines, thrust fronts in the pro-wedge are inactive and the onset of recent normal faulting is contemporaneous (Cosentino et al., 2017) while the fluvial capture and the integration of the intermontane basins into external drainage systems occurred from both side of the wedge. The patterns of normal faulting initiation and divide migration are inconsistent with an eastward slab roll back, as observed in the Northern Apennines. Nevertheless, these patterns could be also explained through a large wavelength uplift. The causes of a such diffuse uplift, large-scale, are still unclear but are compatible with a break in the slab with a consequent cessation of slab-pull force (Faccenna et al., 2014; Fernández-García et al., 2019; Gvirtzman & Nur, 1999; Magni et al., 2013, 2017; van

10.1029/2022TC007461

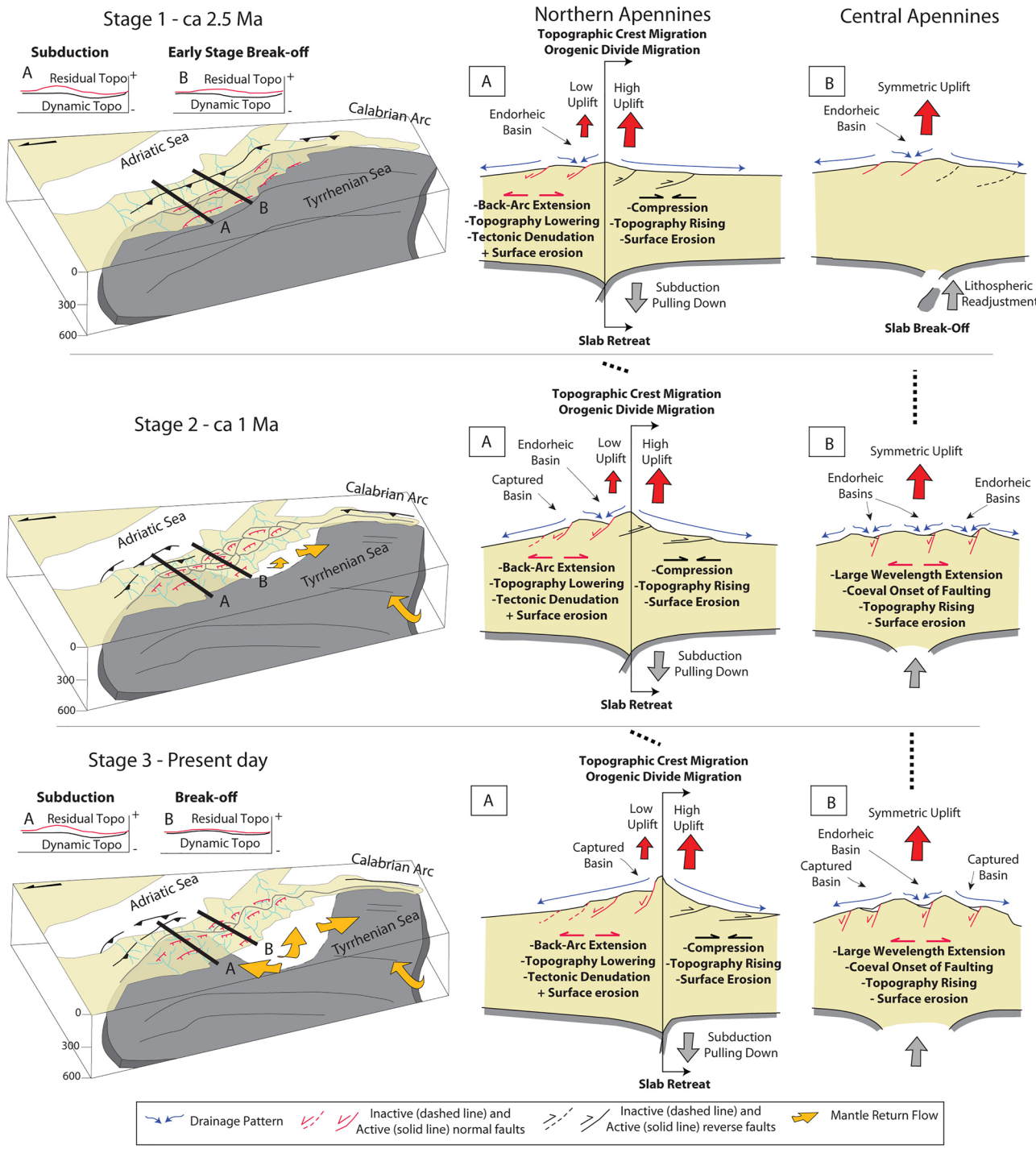

Figure 14. Conceptual model.

Hunen and Allen, 2011; Wortel & Spakman, 2000) (Figure 14). The following lithospheric readjustment and uplift are expected to be quasi-symmetric and centered with respect to the entire width of the wedge. Furthermore, if a break in the slab occurred, it would be expected to be at ca 2.5 Ma, as constrained by the onset of extension, uplift and exhumation (Cosentino et al., 2017; Fellin et al., 2021; San Jose et al., 2020). We then suggest that before the occurrence of slab break-off, the Central Apennines was expected to be structured like the Northern Apennines. After this event, the compression vanished and a large wavelength uplift, centered with respect to the wedge, interested a large area with the formation of normal faults and internally drained, extension-related basins (e.g., Lanari et al., 2021).

7. Conclusion

In this paper we investigated the coupling between topography, crustal and deep mantle structures. We explored how the styles of morphology/deformation and the pattern of exhumation reflect deeper geometry. We gathered into three databases the available low-temperature thermochronological cooling ages, the ages of the youngest lacustrine deposit within intermontane extensional basins and Moho depth estimates from receiver functions (including new data for the Central Apennines). We combined those data with a new qualitative morphometric set of analyses (including k_{sn} drainage areas, longitudinal river profiles and χ plots) that, together with the topographic swath profiles, are used to describe the morphology and to compare (relatively) uplift rates across the Apennines. In addition, we also performed filtering of the topography to infer which processes and associated wavelength are primarily controlling the topographic evolution.

For the first time, our work demonstrates that the geometries of topography and crust are remarkably different along the Apennines that we interpreted as a function of different ongoing geodynamic mechanisms rather than a consequence of lithological variation. Despite this, even if the geodynamic mechanism changes over space, across each single sector of the Apennines, surface, crust, and mantle, share a similar geometry. This coupling between surface, crust and depth processes corresponds to a remarkable asymmetry across the Northern Apennines 1 and 2 and a peculiarly symmetry across the Central and Southern Apennines. This observation has a crucial implication because it demonstrates that along the Apennines, different ongoing mechanisms control the overall geometry of surface, crust, and Moho.

Data Availability Statement

Supporting Information is available at "https://osf.io/kwzb6."

Acknowledgments
The authors thank Maria Giuditta Fellin and Maria Laura Balestrieri for the inspiring discussions. Frank Pazzaglia is warmly acknowledged for the stimulating discussion and for revising the manuscript before submission. We acknowledge the reviewers Jeffrey Park and Nicola D'Agostino for their comments and criticism that improve the manuscript and the editor Duna Roda-Boluda for constructive suggestions. The study was supported by the MIUR (Ministry of Education University and Research), Excellence Department Initiative, Art. 1, com. 314–337, Low 232/2016. And by PRIN 2017–2020 (Geodynamics of the Arabia-Eurasia collisional zones, PI C. Faccenna).

References

Abbate, E., Balestrieri, M. L., Bigazzi, G., Norelli, P., & Quercioli, C. (1994). Fission-track datings and recent rapid denudation in Northern Apennines, Italy. *Memorie della Società Geologica Italiana*, *48*, 579–585.

Amato, V., Aucelli, P. P. C., Cesarano, M., Jicha, B., Lebreton, V., Orain, R., et al. (2014). Quaternary evolution of the largest intermontane basin of the Molise Apennine (central-southern Italy). *Rendiconti Lincei*, *25*(S2), 197–216. https://doi.org/10.1007/s12210-014-0324-y

Amato, V., Aucelli, P. P. C., Cesarano, M., Pappone, G., Rosskopf, C. M., & Ermolli, E. R. (2011). The Sessano intra-montane basin: New multi-proxy data for the Quaternary evolution of the Molise sector of the Central-Southern Apennines (Italy). *Geomorphology*, *128*(1–2), 15–31. https://doi.org/10.1016/j.geomorph.2010.12.019

Angelica, C., Bonforte, A., Distefano, G., Serpelloni, E., & Gresta, S. (2013). Seismic potential in Italy from integration and comparison of seismic and geodetic strain rates. *Tectonophysics*, *608*, 996–1006. https://doi.org/10.1016/j.tecto.2013.07.014

Balestrieri, M. L., Abbate, E., & Bigazzi, G. (1996). Insights on the thermal evolution of the Ligurian Apennines (Italy) through fission-track analysis. *Journal of the Geological Society. London*, *153*(3), 419–425. https://doi.org/10.1144/gsjgs.153.3.0419

Balestrieri, M. L., Bernet, M., Brandon, M. T., Picotti, V., Reiners, P., & Zattin, M. (2003). Pliocene and Pleistocene exhumation and uplift of two key areas of the Northern Apennines. *Quaternary International*, *101*, 67–73. https://doi.org/10.1016/s1040-6182(02)00089-7

Balestrieri, M. L., Pandeli, E., Bigazzi, G., Carosi, R., & Montomoli, C. (2011). Age and temperature constraints on metamorphism and exhumation of the syn-orogenic metamorphic complexes of Northern Apennines, Italy. *Tectonophysics*, *509*(3–4), 254–271. https://doi.org/10.1016/j.tecto.2011.06.015

Balestrieri, M. L., & Ventura, B. (2000). Apatite fissiontrack data and exhumation ages across the main divide of the northern Apennines, Italy. *Eos (Transactions, American Geophysical Union) Fall Meeting Supplement*, *81*(48), T51C-12.

Ballato, P., Landgraf, A., Schildgen, T. F., Stockli, D. F., Fox, M., Ghassemi, M. R., et al. (2015). The growth of a mountain belt forced by base-level fall: Tectonics and surface processes during the evolution of the Alborz Mountains, N Iran. *Earth and Planetary Science Letters*, *425*, 204–218. https://doi.org/10.1016/j.epsl.2015.05.051

Bartolini, C. (2003). When did the Northern Apennine become a mountain chain? *Quaternary International*, *101*, 75–80. https://doi.org/10.1016/s1040-6182(02)00090-3

Bartolini, C., D'Agostino, N., & Dramis, F. (2003). Topography, exhumation, and drainage network evolution of the Apennines. *Episodes*, *26*(3), 212–216. https://doi.org/10.18814/epiiugs/2003/v26i3/010

Basilici, G. (1997). Sedimentary facies in an extensional and deep-lacustrine depositional system: The Pliocene Tiberino Basin. *Central Italy. Sediment. Geol.*, *109*(1–2), 73–94. https://doi.org/10.1016/s0037-0738(96)00056-5

Bennett, R. A., Serpelloni, E., Hreinsdóttir, S., Brandon, M. T., Buble, G., Basic, T., et al. (2012). Syn-convergent extension observed using the RETREAT GPS network, northern Apennines, Italy. *Journal of Geophysical Research*, *117*(B4). https://doi.org/10.1029/2011jb008744

Benoit, M. H., Torpey, M., Liszewski, K., Levin, V., & Park, J. (2011). P and S wave upper mantle seismic velocity structure beneath the northern Apennines: New evidence for the end of subduction. *Geochemistry, Geophysics, Geosystems*, *12*(6). https://doi.org/10.1029/2010gc003428

Benvenuti, M. (2003). Facies analysis and tectonic significance of lacustrine fan-deltaic successions in the Pliocene–Pleistocene Mugello Basin. *Central Italy. Sediment. Geol.*, *157*(3–4), 197–234. https://doi.org/10.1016/s0037-0738(02)00234-8

Bertoldi, R. (1988). Una sequenza palinologica di eta'Rusciniana nei sedimenti lacustri basali del bacino di Aulla-Olivola (Val di Magra). *Rivista Italiana di Paleontologia e Stratigrafia*, *94*.

Bonini, M., Moratti, G., Sani, F., & Balestrieri, M. L. (2013). Compression-to-extension record in the late Pliocene-Pleistocene upper Valdarno basin (northern Apennines, Italy): Structural and thermochronological constraints. *Italian Journal of Geosciences*, *132*(1), 54–80. https://doi.org/10.3301/ijg.2011.18

Bossio, A., Costantini, A., Mazzei, R., Salvatorini, G. F., & Terzuoli, A. (1994). IL Neogene dell'area della Marsiliana (Grosseto).

Bossio, A., Foresi, L. M., Mazzei, R., Salvatorini, G., & Sandrelli, F. (1995). Evoluzione tettonico-sedimentaria neogenica lungo una trasversale ai Bacini di Volterra e della Val d'Elsa.

Carannante, S., Monachesi, G., Cattaneo, M., Amato, A., & Chiarabba, C. (2013). Deep structure and tectonics of the northern-central Apennines as seen by regional-scale tomography and 3-D located earthquakes. *Journal of Geophysical Research: Solid Earth*, *118*(10), 5391–5403. https://doi.org/10.1002/jgrb.50371

Carlini, M., Artoni, A., Aldega, L., Balestrieri, M. L., Corrado, S., Vescovi, P., et al. (2013). Exhumation and reshaping of far-travelled/allochthonous tectonic units in mountain belts. New insights for the relationships between shortening and coeval extension in the western Northern Apennines (Italy). *Tectonophysics*, *608*, 267–287. https://doi.org/10.1016/j.tecto.2013.09.029

Carminati, E., & Doglioni, C. (2012). Alps vs. Apennines: The paradigm of a tectonically asymmetric Earth. *Earth-Science Reviews*, *112*(1–2), 67–96. https://doi.org/10.1016/j.earscirev.2012.02.004

Carminati, E., Doglioni, C., & Scrocca, D. (2004). Alps vs Apennines. *Spec. Vol. The Italian Geological Society IGC*, *32*, 141–151.

Carminati, E., Doglioni, C., & Scrocca, D. (2005). 4. Magnitude and causes of long-term subsidence of. Flooding and environmental challenges for Venice and its lagoon: State of knowledge (Vol. *21*).

Carminati, E., Lustrino, M., Cuffaro, M., & Doglioni, C. (2010). Tectonics, magmatism and geodynamics of Italy: What we know and what we imagine. *Journal of the Virtual Explorer*, *36*(8), 10–3809. https://doi.org/10.3809/jvirtex.2010.00226

Carroll, A. R., & Bohacs, K. M. (1999). Stratigraphic classification of ancient lakes: Balancing tectonic and climatic controls. *Geology*, *27*(2), 99–102. https://doi.org/10.1130/0091-7613(1999)027<0099:scoalb>2.3.co;2

Casero, P. (2004). Structural setting of petroleum exploration plays in Italy. *Spec. Vol. The Italian Geological Society IGC*, *32*, 189–199.

Cavinato, G. P., & Celles, P. G. D. (1999). Extensional basins in the tectonically bimodal central Apennines fold-thrust belt, Italy: Response to corner flow above a subducting slab in retrograde motion. *Geology*, *27*(10), 955–958. https://doi.org/10.1130/0091-7613(1999)027<0955:ebittb>2.3.co;2

Chiarabba, C., Bagh, S., Bianchi, I., De Gori, P., & Barchi, M. (2010). Deep structural heterogeneities and the tectonic evolution of the Abruzzi region (Central Apennines, Italy) revealed by microseismicity, seismic tomography, and teleseismic receiver functions. *Earth and Planetary Science Letters*, *295*(3–4), 462–476. https://doi.org/10.1016/j.epsl.2010.04.028

Chiarabba, C., & Chiodini, G. (2013). Continental delamination and mantle dynamics drive topography, extension and fluid discharge in the Apennines. *Geology*, *41*(6), 715–718. https://doi.org/10.1130/g33992.1

Chiarabba, C., Giacomuzzi, G., Bianchi, I., Agostinetti, N. P., & Park, J. (2014). From underplating to delamination-retreat in the northern Apennines. *Earth and Planetary Science Letters*, *403*, 108–116. https://doi.org/10.1016/j.epsl.2014.06.041

Chiarabba, C., Jovane, L., & DiStefano, R. (2005). A new view of Italian seismicity using 20 years of instrumental recordings. *Tectonophysics*, *395*(3–4), 251–268. https://doi.org/10.1016/j.tecto.2004.09.013

Cimini, G. B., & Marchetti, A. (2006). Deep structure of peninsular Italy from seismic tomography and subcrustal seismicity. *Annals of Geophysics*, *49*(1), 331–345.

Clementucci, R., Ballato, P., Siame, L., Faccenna, C., Yaaqoub, A., Essaifi, A., et al. (2022). Lithological control on erosional dynamics in a tectonically inactive mountain belt (Anti-Atlas, Morocco). *Earth and Planetary Science Letters*, *596*, 117788. https://doi.org/10.1016/j.epsl.2022.117788

Clementucci, R., Ballato, P., Siame, L., Fox, M., Lanari, R., Sembroni, A., et al. (2023). Surface uplift and topographic rejuvenation of a tectonically inactive range: Insights from the Anti-Atlas and the Siroua Massif (Morocco). *Tectonics*, *42*(2), e2022TC007383. https://doi.org/10.1029/2022TC007383

Collettini, C., & Barchi, M. R. (2004). A comparison of structural data and seismic images for low-angle normal faults in the northern Apennines (central Italy): Constraints on activity. *Geological Society, London, Special Publications*, *224*(1), 95–112. https://doi.org/10.1144/gsl.sp.2004.224.01.07

Collettini, C., De Paola, N., Holdsworth, R. E., & Barchi, M. R. (2006). The development and behaviour of low-angle normal faults during Cenozoic asymmetric extension in the Northern Apennines, Italy. *Journal of Structural Geology*, *28*(2), 333–352. https://doi.org/10.1016/j.jsg.2005.10.003

Conticelli, S., Boari, E., Burlamacchi, L., Cifelli, F., Moscardi, F., Laurenzi, M. A., et al. (2015). Geochemistry and Sr-Nd-Pb isotopes of Monte Amiata volcano, central Italy: Evidence for magma mixing between high-K calc-alkaline and leucititic mantle-derived magmas. *Italian Journal of Geosciences*, *134*(2), 266–290. https://doi.org/10.3301/ijg.2015.12

Corrado, S., Aldega, L., Di Leo, P., Giampaolo, C., Invernizzi, C., Mazzoli, S., & Zattin, M. (2005). Thermal maturity of the axial zone of the southern Apennines fold-and-thrust belt (Italy) from multiple organic and inorganic indicators. *Terra Nova*, *17*(1), 56–65. https://doi.org/10.1111/j.1365-3121.2004.00584.x

Cosentino, D., Asti, R., Nocentini, M., Gliozzi, E., Kotsakis, T., Mattei, M., et al. (2017). New insights into the onset and evolution of the central Apennine extensional intermontane basins based on the tectonically active L'Aquila Basin (central Italy). *GSA Bulletin*, *129*(9–10), 1314–1336. https://doi.org/10.1130/b31679.1

Cosentino, D., Cipollari, P., Marsili, P., & Scrocca, D. (2010). Geology of the central Apennines: A regional review. *Journal of the Virtual Explorer*, *36*, 1–37. https://doi.org/10.3809/jvirtex.2010.00223

Coward, M. P., De Donatis, M., Mazzoli, S., Paltrinieri, W., & Wezel, F. (1999). Frontal part of the northern Apennines fold and thrust belt in the Romagna-Marche area (Italy): Shallow and deep structural styles. *Tectonics*, *18*(3), 559–574. https://doi.org/10.1029/1999tc900003

D'Agostino, N., Jackson, J. A., Dramis, F., & Funiciello, R. (2001). Interactions between mantle upwelling, drainage evolution and active normal faulting: An example from the central Apennines (Italy). *Geophysical Journal International*, *147*(2), 475–497. https://doi.org/10.1046/j.1365-246x.2001.00539.x

D'Agostino, N., Mantenuto, S., D'Anastasio, E., Giuliani, R., Mattone, M., Calcaterra, S., et al. (2011). Evidence for localized active extension in the central Apennines (Italy) from global positioning system observations. *Geology*, *39*(4), 291–294. https://doi.org/10.1130/g31796.1

D'Alessandro, L., Miccadei, E., & Piacentini, T. (2003). Morphostructural elements of central–eastern Abruzzi: Contributions to the study of the role of tectonics on the morphogenesis of the Apennine chain. *Quaternary International*, *101*, 115–124. https://doi.org/10.1016/s1040-6182(02)00094-0

De Luca, G., Cattaneo, M., Monachesi, G., & Amato, A. (2009). Seismicity in central and northern Apennines integrating the Italian national and regional networks. *Tectonophysics*, *476*(1–2), 121–135. https://doi.org/10.1016/j.tecto.2008.11.032

Dewey, J. F., Helman, M. L., Knott, S. D., Turco, E., & Hutton, D. H. W. (1989). Kinematics of the western Mediterranean. *Geological Society, London, Special Publications*, *45*(1), 265–283. https://doi.org/10.1144/gsl.sp.1989.045.01.15

Dewey, J. F., Pitman, W. C., III, Ryan, W. B. F., & Bonnin, J. (1973). Plate tectonics and the evolution of the Alpine system. *The Geological Society of America Bulletin*, *84*(10), 3137–3180. https://doi.org/10.1130/0016-7606(1973)84<3137:ptateo>2.0.co;2

Diaferia, G., Cammarano, F., & Faccenna, C. (2019). Thermal structure of a vanishing subduction system: An example of seismically-derived crustal temperature along the Italian peninsula. *Geophysical Journal International*, *219*, 239–247.
Di Bona, M., Lucente, F. P., & Piana Agostinetti, N. (2008). Crustal structure and Moho depth profile crossing the central Apennines (Italy) along the N42° parallel. *Journal of Geophysical Research*, *113*(B12), B12306. https://doi.org/10.1029/2008JB005625
Di Naccio, D., Boncio, P., Brozzetti, F., Pazzaglia, F. J., & Lavecchia, G. (2013). Morphotectonic analysis of the Lunigiana and Garfagnana grabens (northern Apennines, Italy): Implications for active normal faulting. *Geomorphology*, *201*, 293–311. https://doi.org/10.1016/j.geomorph.2013.07.003
Di Stefano, R., Bianchi, I., Ciaccio, M. G., Carrara, G., & Kissling, E. (2011). Three-dimensional Moho topography in Italy: New constraints from receiver functions and controlled source seismology. *Geochemistry, Geophysics, Geosystems*, *12*(9). https://doi.org/10.1029/2011gc003649
Doglioni, C., Harabaglia, P., Merlini, S., Mongelli, F., Peccerillo, A. T., & Piromallo, C. (1999). Orogens and slabs vs. their direction of subduction. *Earth-Science Reviews*, *45*(3–4), 167–208. https://doi.org/10.1016/s0012-8252(98)00045-2
Erlanger, E. D., Fellin, M. G., & Willett, S. D. (2022). Exhumation and erosion of the northern Apennines, Italy: New insights from low-temperature thermochronometers. *Solid Earth*, *13*(2), 347–365. https://doi.org/10.5194/se-13-347-2022
Ermolli, E. R., Sardella, R., Di Maio, G., Petronio, C., & Santangelo, N. (2010). Pollen and mammals from the late Early Pleistocene site of Saticula (Sant'Agata de'Goti, Benevento, Italy). *Quaternary International*, *225*(1), 128–137. https://doi.org/10.1016/j.quaint.2009.06.013
Faccenna, C., & Becker, T. W. (2020). Topographic expressions of mantle dynamics in the Mediterranean. *Earth-Science Reviews*, *209*, 103327. https://doi.org/10.1016/j.earscirev.2020.103327
Faccenna, C., Becker, T. W., Miller, M. S., Serpelloni, E., & Willett, S. D. (2014). Isostasy, dynamic topography, and the elevation of the Apennines of Italy. *Earth and Planetary Science Letters*, *407*, 163–174. https://doi.org/10.1016/j.epsl.2014.09.027
Faccenna, C., Funiciello, F., Civetta, L., D Antonio, M., Moroni, M., & Piromallo, C. (2007). Slab disruption, mantle circulation, and the opening of the Tyrrhenian basins. *Special Paper the Geological Society of America*, *418*, 153.
Faccenna, C., Mattei, M., Funiciello, R., & Jolivet, L. (1997). Styles of back-arc extension in the central Mediterranean. *Terra Nova*, *9*(3), 126–130. https://doi.org/10.1046/j.1365-3121.1997.d01-12.x
Farley, K. A. (2000). Helium diffusion from apatite: General behavior as illustrated by Durango fluorapatite. *Journal of Geophysical Research*, *105*(B2), 2903–2914. https://doi.org/10.1029/1999jb900348
Fellin, M. G., Reiners, P. W., Brandon, M. T., Wüthrich, E., Balestrieri, M. L., & Molli, G. (2007). Thermochronologic evidence for the exhumational history of the Alpi Apuane metamorphic core complex, northern Apennines, Italy. *Tectonics*, *26*(6), TC6015. https://doi.org/10.1029/2006tc002085
Fellin, M. G., San Jose, M., Faccenna, C., Willett, S. D., Cosentino, D., Lanari, R., et al. (2021). Transition from slab roll-back to slab break-off in the central Apennines, Italy: Constraints from the stratigraphic and thermochronologic record. *GSA Bulletin*, *34*, (7–8), 1916–1930. https://doi.org/10.1130/B36123.1
Fernández-García, C., Guillaume, B., & Brun, J.-P. (2019). 3D slab breakoff in laboratory experiments. *Tectonophysics*, *773*, 228223. https://doi.org/10.1016/j.tecto.2019.228223
Ferrarini, F., de Nardis, R., Brozzetti, F., Cirillo, D., Arrowsmith, J. R., & Lavecchia, G. (2021). Multiple lines of evidence for a potentially seismogenic fault along the central-Apennine (Italy) active extensional belt–an unexpected outcome of the MW6. 5 Norcia 2016 earthquake. *Frontiers of Earth Science*, *9*, 490. https://doi.org/10.3389/feart.2021.642243
Ferreli, L., Brunamonte, F., Filippi, G., Margheriti, L., & Michetti, A. M. (1992). Riconoscimento di un livello lacustre della prima eta'del ferro nel bacino di Rieti e possibili implicazioni neotettoniche.
Ficcarelli, G., Abbazzi, L., Albianelli, A., Bertini, A., Coltorti, M., Magnatti, M., et al. (1997). Cesi, an early middle Pleistocene site in the Colfiorito basin (Umbro-Marchean Apennine), central Italy. *Journal of Quaternary Science*, *12*(6), 507–518. https://doi.org/10.1002/(sici)1099-1417(199711/12)12:6<507::aid-jqs329>3.0.co;2-e
Fidolini, F., Ghinassi, M., Magi, M., Papini, M., & Sagri, M. (2013). The Plio-Pleistocene fluvio-lacustrine upper Valdarno basin (central Italy): Stratigraphy and basin fill evolution. *Italian Journal of Geosciences*, *132*(1), 13–32. https://doi.org/10.3301/ijg.2012.06
Fisher, J. A., Pazzaglia, F. J., AnastasioGallen, D. J. S. F. D. J., & Gallen, S. F. (2022). Linear inversion of fluvial topography in the northern Apennines: Comparison of base-level fall to crustal shortening. *Tectonics*, *41*(11), e2022TC007379. https://doi.org/10.1029/2022tc007379
Flint, J. J. (1974). Stream gradient as a function of order, magnitude, and discharge. *Water Resources Research*, *10*(5), 969–973. https://doi.org/10.1029/wr010i005p00969
Forte, A. M., & Whipple, K. X. (2018). Criteria and tools for determining drainage divide stability. *Earth and Planetary Science Letters*, *493*, 102–117. https://doi.org/10.1016/j.epsl.2018.04.026
Geurts, A. H., Cowie, P. A., Duclaux, G., Gawthorpe, R. L., Huismans, R. S., Pedersen, V. K., & Wedmore, L. N. J. (2018). Drainage integration and sediment dispersal in active continental rifts: A numerical modelling study of the central Italian Apennines. *Basin Research*, *30*(5), 965–989. https://doi.org/10.1111/bre.12289
Ghinassi, M., Abbazzi, L., Esu, D., Gaudant, J., & Girotti, O. (2005). Facies analysis, stratigraphy and palaeontology (molluscs and vertebrates) in the Upper Pliocene sandy flood-basin deposits of the Upper Valdarno Basin (Northern Apennines). *Rivista Italiana di Paleontologia e Stratigrafia*, *111*.
Giacomuzzi, G., Civalleri, M., De Gori, P., & Chiarabba, C. (2012). A 3D vs model of the upper mantle beneath Italy: Insight on the geodynamics of central Mediterranean. *Earth and Planetary Science Letters*, *335*, 105–120. https://doi.org/10.1016/j.epsl.2012.05.004
Gioia, D., Schiattarella, M., Mattei, M., & Nico, G. (2011). Quantitative morphotectonics of the Pliocene to quaternary Auletta basin, southern Italy. *Geomorphology*, *134*(3–4), 326–343. https://doi.org/10.1016/j.geomorph.2011.07.009
Goren, L., Fox, M., & Willett, S. D. (2014). Tectonics from fluvial topography using formal linear inversion: Theory and applications to the Inyo Mountains, California. *Journal of Geophysical Research: Earth Surface*, *119*(8), 1651–1681. https://doi.org/10.1002/2014jf003079
Green, P. F., Duddy, I. R., Laslett, G. M., Hegarty, K. A., Gleadow, A. J. W., & Lovering, J. F. (1989). Thermal annealing of fission tracks in apatite 4. Quantitative modelling techniques and extension to geological timescales. *Chemical Geology: Isotope Geoscience section*, *79*(2), 155–182. https://doi.org/10.1016/0168-9622(89)90018-3
Gueguen, E., Doglioni, C., & Fernandez, M. (1998). On the post-25 Ma geodynamic evolution of the western Mediterranean. *Tectonophysics*, *298*(1–3), 259–269. https://doi.org/10.1016/s0040-1951(98)00189-9
Gutscher, M.-A., Baptista, M. A., & Miranda, J. M. (2006). The Gibraltar arc seismogenic zone (Part 2): Constraints on a shallow east dipping fault plane source for the 1755 Lisbon earthquake provided by tsunami modeling and seismic intensity. *Tectonophysics*, *426*(1–2), 153–166. https://doi.org/10.1016/j.tecto.2006.02.025
Gvirtzman, Z., & Nur, A. (1999). Plate detachment, asthenosphere upwelling, and topography across subduction zones. *Geology*, *27*(6), 563–566. https://doi.org/10.1130/0091-7613(1999)027<0563:pdauat>2.3.co;2

Gvirtzman, Z., & Nur, A. (2001). Residual topography, lithospheric structure and sunken slabs in the central Mediterranean. *Earth and Planetary Science Letters*, *187*(1–2), 117–130. https://doi.org/10.1016/s0012-821x(01)00272-2

He, C., Yang, C. J., Turowski, J. M., Rao, G., Roda-Boluda, D. C., & Yuan, X. P. (2021). Constraining tectonic uplift and advection from the main drainage divide of a mountain belt. *Nature Communications*, *12*(1), 544. https://doi.org/10.1038/s41467-020-20748-2

Heidarzadeh, G., Ballato, P., Hassanzadeh, J., Ghassemi, M. R., & Strecker, M. R. (2017). Tectonic and climatic controls on Pliocene sedimentary basin evolution, overspilling and incision of the northwestern Iranian Plateau, Mianeh Basin. *Earth and Planetary Science Letters*, *469*, 135–147. https://doi.org/10.1016/j.epsl.2017.04.019

Iannace, A., Vitale, S., D'errico, M., Mazzoli, S., Di Staso, A., Macaione, E., et al. (2007). The carbonate tectonic units of northern Calabria (Italy): A record of Apulian palaeomargin evolution and Miocene convergence, continental crust subduction, and exhumation of HP–LT rocks. *Journal of the Geological Society. London*, *164*(6), 1165–1186. https://doi.org/10.1144/0016-76492007-017

Ielpi, A. (2011). Geological map of the Santa Barbara basin (northern Apennines, Italy). *Journal of Maps*, *7*(1), 614–625. https://doi.org/10.4113/jom.2011.1181

Invernizzi, C., Bigazzi, G., Corrado, S., Di Leo, P., Schiattarella, M., & Zattin, M. (2008). New thermobaric constraints on the exhumation history of the Liguride accretionary wedge, southern Italy. *Ofioliti*, *33*, 21–32.

Kirby, E., & Ouimet, W. (2011). Tectonic geomorphology along the eastern margin of Tibet: Insights into the pattern and processes of active deformation adjacent to the Sichuan Basin. *Geological Society, London, Special Publications*, *353*(1), 165–188. https://doi.org/10.1144/sp353.9

Kirby, E., & Whipple, K. X. (2012). Expression of active tectonics in erosional landscapes. *Journal of Structural Geology*, *44*, 54–75. https://doi.org/10.1016/j.jsg.2012.07.009

Lanari, R., Boutoux, A., Faccenna, C., Herman, F., Willett, S. D., & Ballato, P. (2023). Cenozoic exhumation in the Mediterranean and the Middle East. *Earth-Science Reviews*, *237*, 104328. https://doi.org/10.1016/j.earscirev.2023.104328

Lanari, R., Faccenna, C., Benedetti, L., Sembroni, A., Bellier, O., Menichelli, I., et al. (2021). Formation and persistence of extensional internally drained basins: The case of the Fucino basin (Central Apennines, Italy). *Tectonics*, *40*(6), e2020TC006442. https://doi.org/10.1029/2020tc006442

Lanari, R., Faccenna, C., Fellin, M. G., Abderrahim, E., Nahid, A., Medina, F., & Youbi, N. (2020). Tectonic evolution of the Western high Atlas of Morocco: Oblique convergence, reactivation and transpression. *Tectonics*, *39*(3), e2019TC005563. https://doi.org/10.1029/2019tc005563

Lanari, R., Fellin, M. G., Faccenna, C., Balestrieri, M. L., Pazzaglia, F., Youbi, N., & Maden, C. (2020). Exhumation and surface evolution of the Western High-Atlas and surrounding regions as constrained by low-temperature thermochronology. *Tectonics*, *39*(3), e2019TC005562. https://doi.org/10.1029/2019tc005562

Lanari, R., Reitano, R., Giachetta, E., Pazzaglia, F. J., Clementucci, R., Faccenna, C., & Fellin, M. G. (2022). Is the Anti-Atlas of Morocco still uplifting? *Journal of African Earth Sciences*, *188*, 104481. https://doi.org/10.1016/j.jafrearsci.2022.104481

Langston, C. A. (1979). Structure under Mount Rainier, Washington, inferred from teleseismic body waves. *Journal of Geophysical Research*, *84*(B9), 4749–4762. https://doi.org/10.1029/jb084ib09p04749

Lucente, F. P., Chiarabba, C., Cimini, G. B., & Giardini, D. (1999). Tomographic constraints on the geodynamic evolution of the Italian region. *Journal of Geophysical Research*, *104*(B9), 20307–20327. https://doi.org/10.1029/1999jb900147

Magni, V., Allen, M. B., van Hunen, J., & Bouilhol, P. (2017). Continental underplating after slab break-off. *Earth and Planetary Science Letters*, *474*, 59–67. https://doi.org/10.1016/j.epsl.2017.06.017

Magni, V., Faccenna, C., van Hunen, J., & Funiciello, F. (2013). Delamination vs. break-off: The fate of continental collision. *Geophysical Research Letters*, *40*(2), 285–289. https://doi.org/10.1002/grl.50090

Malinverno, A., & Ryan, W. B. F. (1986). Extension in the Tyrrhenian Sea and shortening in the Apennines as result of arc migration driven by sinking of the lithosphere. *Tectonics*, *5*(2), 227–245. https://doi.org/10.1029/tc005i002p00227

Malusà, M. G., & Balestrieri, M. L. (2012). Burial and exhumation across the Alps–Apennines junction zone constrained by fission-track analysis on modern river sands. *Terra Nova*, *24*(3), 221–226. https://doi.org/10.1111/j.1365-3121.2011.01057.x

Mancini, M., Vignaroli, G., Bucci, F., Cardinali, M., Cavinato, G. P., Di Salvo, C., et al. (2020). New stratigraphic constraints for the Quaternary source-to-sink history of the Amatrice Basin (central Apennines, Italy). *Geological Journal*, *55*(6), 4226–4251. https://doi.org/10.1002/gj.3672

Manzi, G., Magri, D., Milli, S., Palombo, M. R., Margari, V., Celiberti, V., et al. (2010). The new chronology of the Ceprano calvarium (Italy). *Journal of Human Evolution*, *59*(5), 580–585. https://doi.org/10.1016/j.jhevol.2010.06.010

Marroni, M., Moratti, G., Costantini, A., Conticelli, S., Benvenuti, M. G., Pandolfi, L., et al. (2015). Geology of the Monte Amiata region, southern Tuscany, central Italy. *Italian Journal of Geosciences*, *134*(2), 171–199. https://doi.org/10.3301/ijg.2015.13

Martini, I., Aldinucci, M., Foresi, L. M., Mazzei, R., & Sandrelli, F. (2011). Geological map of the Pliocene succession of the northern Siena basin (Tuscany, Italy). *Journal of Maps*, *7*(1), 193–205. https://doi.org/10.4113/jom.2011.1176

Mazzoli, S., Aldega, L., Corrado, S., Invernizzi, C., & Zattin, M. (2006). Pliocene-quaternary thrusting, syn-orogenic extension and tectonic exhumation in the Southern Apennines (Italy): Insights from the Monte Alpi area. *Special Paper the Geological Society of America*, *414*, 55.

Mazzoli, S., Ascione, A., Buscher, J. T., Pignalosa, A., Valente, E., & Zattin, M. (2014). Low-angle normal faulting and focused exhumation associated with late Pliocene change in tectonic style in the southern Apennines (Italy). *Tectonics*, *33*(9), 1802–1818. https://doi.org/10.1002/2014tc003608

Mazzoli, S., D'errico, M., Aldega, L., Corrado, S., Invernizzi, C., Shiner, P., & Zattin, M. (2008). Tectonic burial and "young"(<10 Ma) exhumation in the southern Apennines fold-and-thrust belt (Italy). *Geology*, *36*(3), 243–246. https://doi.org/10.1130/g24344a.1

Miller, M. S., & Piana Agostinetti, N. (2012). Insights into the evolution of the Italian lithospheric structure from S receiver function analysis. *Earth and Planetary Science Letters*, *345*, 49–59. https://doi.org/10.1016/j.epsl.2012.06.028

Minelli, L., & Faccenna, C. (2010). Evolution of the Calabrian accretionary wedge (central Mediterranean). *Tectonics*, *29*(4). https://doi.org/10.1029/2009tc002562

Molin, P., Fubelli, G., Nocentini, M., Sperini, S., Ignat, P., Grecu, F., & Dramis, F. (2012). Interaction of mantle dynamics, crustal tectonics, and surface processes in the topography of the Romanian Carpathians: A geomorphological approach. *Global and Planetary Change.90–91*, 58–72. https://doi.org/10.1016/j.gloplacha.2011.05.005

Montone, P., Amato, A., & Pondrelli, S. (1999). Active stress map of Italy. *Journal of Geophysical Research*, *104*(B11), 25595–25610. https://doi.org/10.1029/1999jb900181

Montone, P., Mariucci, M. T., & Pierdominici, S. (2012). The Italian present-day stress map. *Geophysical Journal International*, *189*(2), 705–716. https://doi.org/10.1111/j.1365-246x.2012.05391.x

Montone, P., Mariucci, M. T., Pondrelli, S., & Amato, A. (2004). An improved stress map for Italy and surrounding regions (central Mediterranean). *Journal of Geophysical Research*, *109*(B10). https://doi.org/10.1029/2003jb002703

Moodie, A. J., Pazzaglia, F. J., & Berti, C. (2018). Exogenic forcing and autogenic processes on continental divide location and mobility. *Basin Research*, *30*(2), 344–369. https://doi.org/10.1111/bre.12256

Olivetti, V., Laura, B. M., Claudio, F., & Stuart, F. M. (2017). Dating the topography through thermochronology: Application of Pecube code to inverted vertical profile in the eastern Sila Massif, southern Italy. *Italian Journal of Geosciences*, *136*(3), 321–336. https://doi.org/10.3301/ijg.2016.09

Panza, G. F., Peccerillo, A., Aoudia, A., & Farina, B. (2007). Geophysical and petrological modelling of the structure and composition of the crust and upper mantle in complex geodynamic settings: The Tyrrhenian Sea and surroundings. *Earth-Science Reviews*, *80*(1–2), 1–46. https://doi.org/10.1016/j.earscirev.2006.08.004

Papani, G., De Nardo, M. T., Bettelli, G., Rio, D., Tellini, C., & Vernia, L. (2002). Note illustrative della Carta Geologica d'Italia alla scala 1: 50.000.

Patacca, E., Sartori, R., & Scandone, P. (1993). Tyrrhenian basin and Apennines. Kinematic evolution and related dynamic constraints. In *Recent evolution and seismicity of the Mediterranean region* (pp. 161–171). Springer.

Pazzaglia, F. J., & Fisher, J. A. (2022). A reconstruction of Apennine uplift history and the development of transverse drainages from longitudinal profile inversion. In C. Koeberl, P. Claeys, & S. Montanari (Eds.), *From the Guajira desert to the Apennines, and from Mediterranean microplates to the Mexican killer asteroid*, *Geol. Soc. Am. Spec. Pap* (Vol. 557). Geological Society of America.

Pennetta, M., Russo, F., & Donadio, C. (2014). Late Quaternary environmental evolution of the intermontane Valle Caudina basin, southern Italy. *Rendiconti Lincei*, *25*(S2), 231–240. https://doi.org/10.1007/s12210-014-0334-9

Peretto, C., Arnaud, J., Moggi-Cecchi, J., Manzi, G., Nomade, S., Pereira, A., et al. (2015). A human deciduous tooth and new 40Ar/39Ar dating results from the Middle Pleistocene archaeological site of Isernia La Pineta, southern Italy. *PLoS One*, *10*, e0140091. https://doi.org/10.1371/journal.pone.0140091

Perron, J. T., & Royden, L. (2013). An integral approach to bedrock river profile analysis. *Earth Surface Processes and Landforms*, *38*(6), 570–576. https://doi.org/10.1002/esp.3302

Piacentini, T., & Miccadei, E. (2014). The role of drainage systems and intermontane basins in the Quaternary landscape of the Central Apennines chain (Italy). *Rendiconti Lincei*, *25*(S2), 139–150. https://doi.org/10.1007/s12210-014-0312-2

Piana Agostinetti, N., & Amato, A. (2009). Moho depth and Vp/Vs ratio in peninsular Italy from teleseismic receiver functions. *Journal of Geophysical Research*, *114*(B6), B06303. https://doi.org/10.1029/2008jb005899

Piana Agostinetti, N., Buttinelli, M., & Chiarabba, C. (2022). Deep structure of the crust in the area of the 2016-2017 Central Italy seismic sequence from receiver function analysis. *Tectonophysics*, *826*, 229237. https://doi.org/10.1016/j.tecto.2022.229237

Piana Agostinetti, N., & Faccenna, C. (2018). Deep structure of Northern Apennines subduction orogen (Italy) as revealed by a joint interpretation of passive and active seismic data. *Geophysical Research Letters*, *45*(9), 4017–4024. https://doi.org/10.1029/2018gl077640

Piana Agostinetti, N., Steckler, M. S., & Lucente, F. P. (2009). Imaging the subducted slab under the Calabrian Arc, Italy, from receiver function analysisImaging the subducted slab under the Calabrian Arc, Italy. *Lithosphere*, *1*(3), 131–138. https://doi.org/10.1130/l49.1

Picotti, V., Ponza, A., & Pazzaglia, F. J. (2009). Topographic expression of active faults in the foothills of the Northern Apennines. *Tectonophysics*, *474*(1–2), 285–294. https://doi.org/10.1016/j.tecto.2009.01.009

Piromallo, C., & Morelli, A. (2003). P wave tomography of the mantle under the Alpine-Mediterranean area. *Journal of Geophysical Research: Solid Earth*, *108*(B2), 2065. https://doi.org/10.1029/2002jb001757

Pucci, S., De Martini, P. M., Pantosti, D., & Valensise, G. (2003). Geomorphology of the Gubbio basin (central Italy): Understanding the active tectonics and earthquake potential. *Annals of Geophysics*.

Pucci, S., Mirabella, F., Pazzaglia, F., Barchi, M. R., Melelli, L., Tuccimei, P., et al. (2014). Interaction between regional and local tectonic forcing along a complex Quaternary extensional basin: Upper Tiber Valley, Northern Apennines, Italy. *Quaternary Science Reviews*, *102*, 111–132. https://doi.org/10.1016/j.quascirev.2014.08.009

Reitano, R., Faccenna, C., Funiciello, F., Corbi, F., Sternai, P., Willett, S. D., et al. (2022). Sediment recycling and the evolution of analogue orogenic wedges. *Tectonics*, *41*, e2021TC006951. https://doi.org/10.1029/2021TC006951

Rosenbaum, G., & Piana Agostinetti, N. (2015). Crustal and upper mantle responses to lithospheric segmentation in the northern Apennines. *Tectonics*, *34*(4), 648–661. https://doi.org/10.1002/2013tc003498

Royden, L., & Faccenna, C. (2018). Subduction orogeny and the late Cenozoic evolution of the Mediterranean arcs. *Annual Review of Earth and Planetary Sciences*, *46*(1), 261–289. https://doi.org/10.1146/annurev-earth-060115-012419

Royden, L. H. (1993). Evolution of retreating subduction boundaries formed during continental collision. *Tectonics*, *12*(3), 629–638. https://doi.org/10.1029/92tc02641

Rusciadelli, G., Viandante, M. G., Calamita, F., & Cook, A. C. (2005). Burial-exhumation history of the central Apennines (Italy), from the foreland to the chain building: Thermochronological and geological data. *Terra Nova*, *17*(6), 560–572. https://doi.org/10.1111/j.1365-3121.2005.00649.x

Sabato, L., Bertini, A., Masini, F., Albianelli, A., Napoleone, G., & Pieri, P. (2005). The lower and middle Pleistocene geological record of the San Lorenzo lacustrine succession in the Sant'Arcangelo basin (southern Apennines, Italy). *Quaternary International*, *131*(1), 59–69. https://doi.org/10.1016/j.quaint.2004.07.001

San Jose, M., Rugenstein, J. K. C., Cosentino, D., Faccenna, C., Fellin, M. G., Ghinassi, M., & Martini, I. (2020). Stable isotope evidence for rapid uplift of the central Apennines since the late Pliocene. *Earth and Planetary Science Letters*, *544*, 116376. https://doi.org/10.1016/j.epsl.2020.116376

Savastano, L., & Piana Agostinetti, N. (2019). Deep structure of the Southern Apennines as imaged by active and passive seismic data along the CROP-04 (crustal) reflection seismic profile. *Journal of the Geological Society. London*, *176*(6), 1284–1290. https://doi.org/10.1144/jgs2018-201

Serpelloni, E., Faccenna, C., Spada, G., Dong, D., & Williams, S. D. P. (2013). Vertical GPS ground motion rates in the Euro-Mediterranean region: New evidence of velocity gradients at different spatial scales along the Nubia-Eurasia plate boundary. *Journal of Geophysical Research: Solid Earth*, *118*(11), 6003–6024. https://doi.org/10.1002/2013jb010102

Siravo, G., Fellin, M. G., Faccenna, C., Bayona, G., Lucci, F., Molin, P., & Maden, C. (2018). Constraints on the Cenozoic deformation of the northern eastern Cordillera, Colombia. *Tectonics*, *37*(11), 4311–4337. https://doi.org/10.1029/2018tc005162

Snyder, N. P., Whipple, K. X., Tucker, G. E., & Merritts, D. J. (2000). Landscape response to tectonic forcing: Digital elevation model analysis of stream profiles in the Mendocino triple junction region, northern California. *The Geological Society of America Bulletin*, *112*(8), 1250–1263. https://doi.org/10.1130/0016-7606(2000)112<1250:lrttfd>2.0.co;2

Thomson, S. N. (1994). Fission track analysis of the crystalline basement rocks of the Calabrian arc, southern Italy: Evidence of Oligo-Miocene late-orogenic extension and erosion. *Tectonophysics*, *238*(1–4), 331–352. https://doi.org/10.1016/0040-1951(94)90063-9

Thomson, S. N., Brandon, M. T., Reiners, P. W., Zattin, M., Isaacson, P. J., & Balestrieri, M. L. (2010). Thermochronologic evidence for orogen-parallel variability in wedge kinematics during extending convergent orogenesis of the northern Apennines, Italy. *Bulletin*, *122*(7–8), 1160–1179. https://doi.org/10.1130/b26573.1

van Hunen, J., & Allen, M. B. (2011). Continental collision and slab break-off: A comparison of 3-D numerical models with observations. *Earth and Planetary Science Letters*, *302*(1–2), 27–37. https://doi.org/10.1016/j.epsl.2010.11.035

Ventura, B., Pini, G. A., & Zuffa, G. G. (2001). Thermal history and exhumation of the northern Apennines (Italy): Evidence from combined apatite fission track and vitrinite reflectance data from foreland basin sediments. *Basin Research*, *13*(4), 435–448. https://doi.org/10.1046/j.0950-091x.2001.00159.x

Vignaroli, G., Minelli, L., Rossetti, F., Balestrieri, M. L., & Faccenna, C. (2012). Miocene thrusting in the eastern Sila Massif: Implication for the evolution of the Calabria-Peloritani orogenic wedge (southern Italy). *Tectonophysics*, *538*, 105–119. https://doi.org/10.1016/j.tecto.2012.03.011

Villani, F., & Pierdominici, S. (2010). Late quaternary tectonics of the Vallo di Diano basin (southern Apennines, Italy). *Quaternary Science Reviews*, *29*(23–24), 3167–3183. https://doi.org/10.1016/j.quascirev.2010.07.003

Villani, F., Tulliani, V., Sapia, V., Fierro, E., Civico, R., & Pantosti, D. (2015). Shallow subsurface imaging of the Piano di Pezza active normal fault (central Italy) by high-resolution refraction and electrical resistivity tomography coupled with time-domain electromagnetic data. *Geophysical Supplements to the Monthly Notices of the Royal Astronomical Society*, *203*(3), 1482–1494. https://doi.org/10.1093/gji/ggv399

Whipple, K. X., & Tucker, G. E. (1999). Dynamics of the stream-power river incision model: Implications for height limits of mountain ranges, landscape response timescales, and research needs. *Journal of Geophysical Research*, *104*(B8), 17661–17674. https://doi.org/10.1029/1999jb900120

Willett, S. D., & Brandon, M. T. (2002). On steady states in mountain belts. *Geology*, *30*(2), 175–178. https://doi.org/10.1130/0091-7613(2002)030<0175:ossimb>2.0.co;2

Willett, S. D., McCoy, S. W., Perron, J. T., Goren, L., & Chen, C.-Y. (2014). Dynamic reorganization of river basins. *Science*, *80*(6175), 343. https://doi.org/10.1126/science.1248765

Wobus, C., Whipple, K. X., Kirby, E., Snyder, N., Johnson, J., Spyropolou, K., et al. (2006). Tectonics from topography: Procedures, promise, and pitfalls. *Special Paper the Geological Society of America*, *398*, 55.

Wobus, C. W., Tucker, G. E., & Anderson, R. S. (2010). Does climate change create distinctive patterns of landscape incision? *Journal of Geophysical Research: Earth Surface*, *115*(F4), F04008. https://doi.org/10.1029/2009jf001562

Wortel, M. J. R., & Spakman, W. (2000). Subduction and slab detachment in the Mediterranean-Carpathian region. *Science*, *290*(5498), 1910–1917. https://doi.org/10.1126/science.290.5498.1910

Zattin, M., Picotti, V., & Zuffa, G. G. (2002). Fission-track reconstruction of the front of the Northern Apennine thrust wedge and overlying Ligurian unit. *American Journal of Science*, *302*(4), 346–379. https://doi.org/10.2475/ajs.302.4.346

Zembo, I. (2010). Stratigraphic architecture and quaternary evolution of the Val d'Agri intermontane basin (Southern Apennines, Italy). *Sedimentary Geology*, *223*(3–4), 206–234. https://doi.org/10.1016/j.sedgeo.2009.11.011

Zhu, H., Bozdağ, E., Peter, D., & Tromp, J. (2012). Structure of the European upper mantle revealed by adjoint tomography. *Nature Geoscience*, *5*(7), 493–498. https://doi.org/10.1038/ngeo1501